Published in final edited form as:
Traffic. 2014 October ; 15(10): 1099–1121. doi:10.1111/tra.12194.

AP-1A controls secretory granule biogenesis and trafficking of membrane secretory granule proteins

Mathilde Bonnemaison[*], **Nils Bäck**[†], **Yimo Lin**[‡], **Juan S. Bonifacino**[‡], **Richard Mains**[§], and **Betty Eipper**[*,§]

[*]Department of Molecular Biology and Biophysics, University of Connecticut Health Center, Farmington, CT 06030, USA [†]Institute of Biomedicine/Anatomy, University of Helsinki, FIN-00014, Helsinki, Finland [‡]Cell Biology and Metabolism Program, Eunice Kennedy Shriver National Institute of Child Health and Human Development, National Institutes of Health, Bethesda, MD 20892, USA [§]Department of Neuroscience, University of Connecticut Health Center, Farmington, CT 06030, USA

Abstract

The adaptor protein 1A complex (AP-1A) transports cargo between the *trans*-Golgi network (TGN) and endosomes. In professional secretory cells, AP-1A also retrieves material from immature secretory granules (SGs). The role of AP-1A in SG biogenesis was explored using AtT-20 corticotrope tumor cells expressing reduced levels of the AP-1A μ1A subunit. A two-fold reduction in μ1A resulted in a decrease in TGN cisternae and immature SGs and the appearance of regulated secretory pathway components in non-condensing SGs. Although basal secretion of endogenous SG proteins was unaffected, secretagogue-stimulated release was halved. The reduced μ1A levels interfered with the normal trafficking of carboxypeptidase D (CPD) and peptidylglycine α-amidating monooxygenase-1 (PAM-1), integral membrane enzymes that enter immature SGs. The non-condensing SGs contained POMC products and PAM-1, but not CPD. Based on metabolic labeling and secretion experiments, the cleavage of newly synthesized PAM-1 into PHM was unaltered, but PHM basal secretion was increased in sh-μ1A PAM-1 cells. Despite lacking a canonical AP-1A binding motif, yeast two-hybrid studies demonstrated an interaction between the PAM-1 cytosolic domain and AP-1A. Co-immunoprecipitation experiments with PAM-1 mutants revealed an influence of the luminal domains of PAM-1 on this interaction. Thus, AP-1A is crucial for normal SG biogenesis, function and composition.

Corresponding author: Betty A. Eipper, 263 Farmington Ave., Farmington, CT 06030, USA, Phone: 860-679-8898, Fax: 860-678-1885, eipper@uchc.edu.

Supplemental Material

Supplemental Figure 1 is associated with Figure 1 and with Materials and Methods. It shows how quantification of immunofluorescence images was done. The Golgi markers used are validated. Data for PAM-1 cells comparing AP-1A and POMC/ACTH distribution are shown.

Supplemental Figure 2 is associated with Figures 2 and 3; quantification of immunofluorescence images was used to show that μ1A knockdown altered the distribution of POMC/ACTH, PAM and carboxypeptidase D. Quantification of the rescue experiment is also shown.

The authors declare they have no conflicts of interest.

Keywords

regulated secretion; PAM; TGN; peptide hormone; carboxypeptidase D

Introduction

Pituitary endocrine cells, islet β-cells and peptidergic neurons store bioactive peptides in mature secretory granules (SGs) and release them upon stimulation. SG biogenesis starts in the *trans*-most cisterna of the Golgi and requires acquisition of the appropriate peptide precursors, processing enzymes, granule membrane proteins and cytosolic machinery for trafficking to the plasma membrane and regulated exocytosis. The mildly acidic pH and high calcium concentration in the lumen of the *trans*-Golgi network (TGN), along with the properties of the soluble content proteins, contribute to their aggregation and association with lipid rafts and cholesterol-rich membranes (1–4). Integral membrane proteins cannot aggregate as extensively and SG entry by the vesicular monoamine transporter, phogrin, carboxypeptidase D (CPD) and peptidylglycine α-amidating monooxygenase (PAM) involves both luminal and cytosolic domain signals (5–9).

The process of SG formation is poorly understood, but early observations in pituitary lactotropes, pancreatic β-cells and AtT-20 corticotrope tumor cells revealed clathrin coats on the *trans*-most cisterna of the Golgi and on immature SGs, the vesicular compartments formed from these cisternae (10). Members of the adaptor protein (AP) complex family interact with the heavy chain of clathrin and membrane proteins to form clathrin coats. These complexes bind specific membrane cargo proteins and localize to different regions of the cell (11–14). Each member of the AP family (AP-1 through AP-5) is composed of two large subunits (γ/α/δ/ε/ξ, and β1-5), a medium subunit (μ1-5) and a small subunit (σ1-5). AP-1A (γ/β1/μ1A/σ1) is concentrated in the TGN area and on endosomes, where it binds the cytosolic tails of transmembrane protein cargo, facilitating their entry into budding vesicles (15–17). AP-1 interacts directly with clathrin (15,17), and mediates the transport of cargo between the TGN and endosomes (16). Cargo recognition by AP-1A is mediated by the μ1A subunit, which binds a tyrosine-based sorting signal (YXXΦ, where X is any residue and Φ is a hydrophobic residue), and by the γ/σ1 interface, which interacts with a dileucine-based sorting signal ([D/E]XXXL[L/I]) (18–20). The interaction of cargo proteins with AP-1 affects its oligomerization and coordination of the sorting process (16).

Immature SGs are not responsive to secretagogues (21). It is clear that AP-1A plays an essential role in the maturation process that leads to secretagogue responsiveness. The removal of VAMP4, furin and mannose-6-phosphate receptors from immature SGs involves AP-1A binding motifs in their cytosolic domains (22). During the maturation process, soluble content proteins are also removed from immature SGs; these soluble proteins undergo basal or constitutive-like secretion (4,23,24). For prohormones like pro-opiomelanocortin (POMC) and pro-brain derived neurotrophic factor, the more highly processed products released from mature SGs have biological effects distinct from their basally secreted precursors (25,26), making the balance between basal and stimulated secretion an important variable.

Although SGs play an essential role in many endocrine systems, the endocrine consequences of limited AP-1A function have not been explored. Yeast lacking AP-1 and AP-2 are viable (11), but mice lacking γ-adaptin die before implantation and mice lacking μ1A develop only until E13.5 (16,27). Growth is stunted in mice heterozygous for γ-adaptin (27) and patients with mutations in *PREPL*, which binds to μ1A and regulates AP-1A recycling, exhibit growth retardation and anorexia (28). In hippocampal neurons, AP-1A plays a key role in excluding somatodendritic proteins from the SGs that enter axons (29). Genetic studies demonstrate a role for AP-1A in the biogenesis of "glue granules" in the larval salivary gland of *Drosophila* (30), secretory lysosomal granules (rhoptries) in *Toxoplasma gondii* (31) and Weibel-Palade bodies in endothelial cells (32). AP-1 plays an essential role in melanosome biogenesis and in delivering cargo from endosomes to maturing melanosomes, a lysosome-related organelle that stores pigment in melanocytes (33).

AtT-20 corticotrope tumor cells have served as a model system in which to explore SG biogenesis and maturation (34–37). The behavior of soluble granule content proteins can be assessed by monitoring POMC and prohormone convertase 1 (PC1) processing and secretion. The behavior of SG membrane proteins can be assessed by monitoring CPD, which enters immature SGs but is removed during SG maturation (6). AtT-20 lines stably expressing PAM-1 provide another means of monitoring the behavior of a SG membrane protein that catalyzes one of the final modifications in peptide processing. A SG-specific cleavage in its luminal domain makes it possible to monitor PAM-1 entry into immature SGs (38). Although the cytosolic domain of PAM (PAM-CD) affects its trafficking, it is important to note that its two luminal domains each enter immature SGs efficiently on their own (38,39).

To investigate the role of AP-1A in SG biogenesis, expression of its medium subunit, μ1A, was reduced in AtT-20 corticotrope tumor cells and in AtT-20 cells expressing exogenous PAM-1 (PAM-1 cells). PAM-CD lacks a consensus site for interacting with AP-1A, but metabolic labeling studies suggest that PAM-1 is retrieved from immature SGs (40), a process that generally involves AP-1A.

Results

Down-regulation of the medium subunit of AP-1A in PAM-1 cells alters TGN morphology

We first compared the localization of AP-1A and adrenocorticotropic hormone (ACTH), an accepted marker for the regulated secretory pathway, in PAM-1 cells (Figure 1A) (39,41,42). AP-1A was visualized using an antibody for γ-adaptin. Use of an ACTH antibody that recognizes its precursors (referred to as POMC/ACTH staining) allowed visualization of the entire regulated secretory pathway. In PAM-1 cells, POMC products accumulate in the perinuclear TGN area, while tip staining corresponds to mature SGs (open arrowhead in Figure 1A) (39,43,44). As expected, γ-adaptin staining was concentrated in the same perinuclear region, with little γ-adaptin staining at the tips of processes (Figure 1A). For our immunofluorescence studies, we distinguished three regions: the perinuclear region containing the Golgi (which can be demarcated using antisera to TGN38, PAM or GM130) (Supplemental Figures 1A and B), the tips of processes and the intervening region (referred to as intermediate). Signal intensity in each region was quantified (see Materials and

Methods), confirming the enrichment of POMC/ACTH, but not of γ-adaptin, at the tips of processes (Supplemental Figures 1A and 1C). Vesicular staining for POMC/ACTH and γ-adaptin was observed throughout the region between the Golgi and the tips; although the POMC/ACTH and γ-adaptin staining patterns in this intermediate region clearly differed, the intensity ratios for POMC/ACTH and γ-adaptin staining in the intermediate region vs. the Golgi region were similar (Supplemental Figure 1C).

SG biogenesis begins at the TGN, where both γ-adaptin and POMC/ACTH are located. To test the hypothesis that AP-1A is necessary for SG formation and maturation, we generated PAM-1 cells with reduced levels of μ1A; μ1A was selected as our target because its cargo recognition motifs are known (18–20). Lentiviruses encoding shRNAs targeted to five regions of μ1A mRNA were used to generate multiple stable cell lines (see Material and Methods). Infected PAM-1 cells were selected using puromycin and μ1A levels were determined by Western blot analysis. In PAM-1 cells infected with lentivirus #549 (sh-μ1A PAM-1 cells), μ1A levels were reduced to 50% of their normal value, the greatest effect observed. Removal of one subunit of the AP-1A core complex alters the stability of the remaining complex (45); consistent with this, levels of other AP-1A subunits are reduced in fibroblasts lacking μ1A (16,27). To see whether a similar effect was observed in PAM-1 cells, γ-adaptin levels were quantified; levels of γ-adaptin in sh-μ1A PAM-1 cells were 80% ± 4% of control values (data not shown). Cells infected with a lentivirus encoding a non-target shRNA were used as a control (scramble PAM-1 cells) (Figure 1B). The morphology of sh-μ1A and scramble PAM-1 cells was not consistently different.

To resolve the complex cisternal and vacuolar structures in the TGN region and the small, punctate structures observed with AP-1A and POMC/ACTH immunofluorescent staining, we turned to transmission electron microscopy and compared the morphology of the TGN in scramble and sh-μ1A PAM-1 cells (Figure 1C). The TGN was defined as the tubulovesicular cellular domain at the trans-side of the Golgi stack, bordered by endoplasmic reticulum and mitochondria. This domain corresponds to the distribution of the TGN marker syntaxin 6 and the steady state distribution of PAM in these cells; the distribution of the TGN marker TGN38 is more restricted within this domain (39,46). Stereological analyses of the Golgi stacks revealed no difference in stack membrane area (Figure 1Ca) and the percentage of the whole Golgi volume fraction attributed to the TGN was not different in the two cell lines (Figure 1Cb). However, the surface area of TGN cisternal membranes decreased in sh-μ1A PAM-1 cells compared to scramble PAM-1 cells; pronounced vacuolization of the TGN was observed in sh-μ1A PAM-1 cells (Figure 1Cc).

When newly synthesized SG content proteins reach the TGN, the decreased luminal pH and increased calcium concentration facilitate the formation of aggregates, which must acquire membrane of the appropriate composition before budding from the TGN to form immature SGs (4,47). To investigate this process, immature and mature SGs were examined in scramble and sh-μ1A PAM-1 cells.

The formation of immature SGs is impaired in sh-μ1A PAM-1 cells

SGs in scramble and sh-μ1A PAM-1 cells were first analyzed using the POMC/ACTH antibody; the Golgi region was visualized using antibody to GM130, a *cis*-Golgi marker,

(Figure 2A); as expected from the TGN and endosomal localization and function of AP-1A, the steady state distribution of GM130 was unaltered in scramble and sh-μ1A PAM-1 cells. POMC/ACTH positive puncta accumulated at the tips of processes in both cell types; the ratio of tip to Golgi area POMC/ACTH signal intensities did not differ between scramble and sh-μ1A PAM-1 cells (Figure 2A and Supplemental Figure 2A). However, the POMC/ACTH-positive puncta located between the Golgi/TGN region and the tips differed in sh-μ1A PAM-1 cells. Instead of the evenly distributed, small POMC/ACTH-positive puncta observed in scramble PAM-1 cells, a smaller number of what appeared to be larger and more scattered POMC/ACTH positive puncta were observed in sh-μ1A PAM-1 cells (red arrows in Figure 2A). The ratio of intermediate to Golgi POMC/ACTH signal intensities decreased by 40% in sh-μ1A PAM-1 cells compared to scramble PAM-1 cells (Supplemental Figure 2A).

To understand why POMC/ACTH staining differed in scramble vs sh-μ1A PAM-1 cells, we turned to transmission electron microscopy. Mature SGs of similar appearance were observed at the tips of cellular processes in both cell lines (Figure 2B, left). Immature SGs can be distinguished from mature SGs in these cells by their localization in the TGN area and their electron dense core surrounded by an electron lucent halo. The number of immature SGs in the TGN area decreased by 50% in sh-μ1A PAM-1 cells (Figure 2B).

In sh-μ1A PAM-1 cells, vacuolar structures were common in the region between the Golgi complex and the surrounding plasma membrane (Figures 1C and 2C). In contrast to the high density consistently observed in mature SGs, the electron density of these vacuolar structures varied from lucent to moderately dense. Vacuoles located in a 500 nm peripheral zone of cytoplasm overlying the Golgi complex were counted in scramble and sh-μ1A PAM-1 cells; their number increased almost three-fold in sh-μ1A PAM-1 cells (Figure 2C).

Since a decrease in the number of immature SGs and the appearance of these vacuolar structures were the most dramatic morphological changes observed in response to reducing levels of μ1A, we hypothesized that these vacuolar structures derived from the regulated secretory pathway. We thus searched for additional markers that could be used to characterize them.

Diminished levels of μ1A result in altered localization of PAM and CPD

Immature SGs contain proteins targeted to mature SGs along with proteins that function in the regulated secretory pathway but are removed during the maturation process. Since PAM-1 and CPD fall into this category (40,48), we used immunofluorescence to determine whether reducing μ1A expression altered their localization. We visualized PAM-1 and GM130 in scramble and sh-μ1A PAM-1 cells (Figure 3A). As expected, using an antiserum to its C-terminus, PAM-1 was found in the perinuclear Golgi region identified by GM130 and in vesicular structures distributed throughout the cell (39). Quantification of PAM-staining intensities in the tips vs. the Golgi region did not differ (Supplemental Figure 2B). As observed for POMC/ACTH staining (Figure 2A and Supplemental Figure 2A), bright PAM-positive puncta located between the Golgi/TGN region and the tips of processes were prevalent in sh-μ1A cells (red arrows in Figure 3A). The ratio of intermediate to Golgi PAM

signal intensities decreased by 30% in sh-μ1A PAM-1 cells compared to scramble PAM-1 cells (Supplemental Figure 2B).

CPD, which removes Arg or Lys residues from the C-terminus of proteins and peptides, enters immature SGs but is absent from mature SGs (48). Despite lacking an AP binding motif, *in vitro* studies demonstrated that its cytosolic domain (CPD-CD) interacts with AP-1A and AP-2 (6). In scramble PAM-1 cells, endogenous CPD localized to the Golgi (GM130) area, with some staining of nearby vesicles (Figure 3B). A clear change in CPD localization occurred in sh-μ1A PAM-1 cells; CPD was more prevalent in vesicles distributed throughout the cytoplasm. The ratio of intermediate to Golgi CPD signal intensities increased almost 3-fold in sh-μ1A PAM-1 cells (Supplemental Figure 2C). Decreasing the levels of μ1A in HeLa cells resulted in a similar shift in the localization of a CD8/CPD chimera (49).

We took advantage of the dramatic difference in CPD localization observed in sh-μ1A cells to verify that the phenotype could be reversed by expressing mCherry-μ1A*, in which the coding sequence was mutated to make the fluorescently-tagged protein resistant to the shRNA #549. CPD was visualized in sh-μ1A PAM-1 cells transiently expressing mCherry-μ1A* (Figure 3C). Transfected sh-μ1A PAM-1 cells expressed varying levels of mCherry-μ1A*. Only sh-μ1A PAM-1 cells expressing mCherry-μ1A* whose distribution resembled that of γ-adaptin (Figure 1A) were used for the analysis; in these cells, the endogenous CPD was concentrated in the perinuclear region, as seen in scramble PAM-1 cells. Average intensity of intermediate over Golgi ratios from transfected and non-transfected cells showed an almost 50% decrease in cells transfected with the rescue plasmid. sh-μ1A PAM-1 cells expressing high levels of the construct showed a diffuse mCherry-μ1A* distribution and were excluded from the analysis (not shown). These data confirmed that the phenotype observed in sh-μ1A PAM-1 cells was due to the diminished levels of μ1A.

Reducing the levels of μ1A in PAM-1 cells altered the localization of three regulated secretory pathway markers, POMC/ACTH, PAM and CPD. To find out whether the vacuolar structures that appeared in the sh-μ1A PAM-1 cells derived from the regulated secretory pathway, we turned to immunoelectron microscopy using these three marker proteins.

ACTH and PAM accumulate in the vacuolar structures that appear in sh-μ1A PAM-1 cells

POMC endoproteolytic cleavage generates multiple products (Figure 4A). The initial cleavage occurs at the C-terminus of ACTH; although detectable in the TGN, this cleavage occurs primarily in immature SGs. An antiserum specific for the C-terminus of ACTH and unable to cross-react with POMC allowed identification of cleaved product (42). Using immunoelectron microscopy, we previously identified PAM-1 in the TGN cisternae, mature SGs and multivesicular bodies of PAM-1 cells (46). Cisternal structures in the TGN area of scramble and sh-μ1A PAM-1 cells did not differ from the same structures in PAM-1 cells; an accumulation of PAM protein was apparent (Figure 4B, left). The morphology of the PAM-1 positive SGs at the tips of scramble and sh-μ1A PAM-1 cells did not differ; in both cell lines, staining for ACTH was concentrated in these structures (Figure 4B, right).

To determine whether the vacuoles observed in sh-μ1A PAM-1 cells (Figure 2C) derived from the regulated secretory pathway, ACTH and PAM-1 were visualized simultaneously (Figure 4C). The vacuolar structures were enriched in both ACTH and PAM; as expected, the multivesicular bodies (MVBs) in the sh-μ1A cells contained PAM, but did not contain ACTH. The vacuoles did not accumulate at the tips of processes, where mature SGs accumulated (Figure 4C, left). The presence of ACTH in these vacuolar structures identified them as a derivative of the regulated pathway. The vacuoles lack the high electron density consistently observed in immature and mature SGs, suggesting a lack of content condensation and are tentatively referred to as non-condensing SGs.

To determine whether these vacuolar structures were part of the endosomal system, we assessed the ability of wheat germ agglutinin (WGA) tagged with horseradish peroxidase (HRP) to enter them. The sh-μ1A PAM-1 cells were incubated with tagged WGA for 10 minutes at 37°C; cells were then fixed and stained for HRP (Figure 4D). WGA-HRP was readily detected on the plasma membrane and in early endosomes; it was not, however, apparent in the vacuolar structures. The vacuolar structures that appear near the plasma membrane in the region of the cell that contains the Golgi complex in cells with reduced μ1A levels are therefore referred to as non-condensing SGs.

Like PAM-1, CPD was located in cisternal and vacuolar structures in the TGN area of scramble PAM-1 cells (Figure 4Ea). Double staining for CPD and ACTH confirmed their co-localization in immature SGs in the TGN area of scramble PAM-1 cells (Figure 4Eb). Very few mature SGs in scramble or sh-μ1A PAM-1 cells contained CPD (Figure 4Ec and 4Ef). In the TGN area of sh-μ1A PAM-1 cells, CPD was identified in cisternal structures rather than vacuolar structures (Figure 4Ed) and was absent from immature SGs containing PAM (Figure 4Ee). Very few of the PAM containing non-condensing SGs found in sh-μ1A PAM-1 cells contained CPD (Figure 4Eg); instead, CPD was localized in small vesicular or tubular structures generally devoid of PAM (Figure 4Eh). Immunofluorescent and immuno-EM staining indicated that the trafficking of PAM-1 and CPD responded very differently to reduced μ1A levels. To evaluate the functional consequences of these morphological changes, the cleavage of SG proteins and their basal and stimulated secretion were assessed.

Regulated secretion of soluble SG proteins is impaired in sh-μ1A cells

The non-condensing SGs that appeared in sh-μ1A PAM-1 cells contain ACTH and PAM and would be expected to contain prohormone convertase 1 (PC1), a soluble SG component (50–52). Based on previous studies, analysis of PC1 and POMC products provides a means of distinguishing secretion from immature vs. mature SGs (53). PC1 is synthesized as an 87 kDa precursor (proPC1); autoproteolytic cleavage in the endoplasmic reticulum generates an 81 kDa intermediate (Figure 5A). When exiting the TGN, 81 kDa PC1 is cleaved to generate a more active 63 kDa form. While 81 kDa PC1 is secreted basally, secretion of 63 kDa PC1 is secretagogue responsive. Using an antibody which recognizes all three forms of PC1, no significant differences were observed in the steady state levels of these PC1 cleavage products in the three cell lines (Figure 5B).

In order to determine whether the content of these non-condensing SGs was stored or released rapidly into the medium, we assessed secretion using a simple stimulation

paradigm. Duplicate wells of cells were exposed to control medium or to medium containing 2 mM $BaCl_2$, a mimic of calcium that causes sustained secretion of mature SGs (54). As expected, proPC1 (87 kDa) was not detected in the medium. The 81 kDa form of PC1, which is not stored in mature SGs, was secreted at a similar rate by all three cell lines. The 63 kDa form of PC1 is stored in mature SGs; stimulation with $BaCl_2$ produced a significant increase in its secretion in all three cell lines. Basal secretion of 63 kDa PC1 was not altered in sh-μ1A PAM-1 cells but $BaCl_2$ stimulated secretion of 63 kDa PC1 was significantly diminished (Figure 5C). These data indicate that the decrease in μ1A levels observed in sh-μ1A PAM-1 cells was sufficient to impair SG maturation.

Since AtT-20 cells are specialized in producing and storing ACTH, we next asked whether POMC processing and secretion was altered when μ1A levels were reduced. In order to generalize our observations beyond the PAM-1 cell line and since exogenous expression of PAM-1 alters cytoskeletal organization and limits POMC processing and secretion (44), we addressed this question using wild-type (wt) AtT-20 cells; wt AtT-20 cells were infected with the non-target virus (scramble wt) or the #549 virus (sh-μ1A wt) and multiple stable cell lines were selected. Levels of μ1A were reduced by about 40% in the sh-μ1A wt lines (Figure 6A).

In addition to ACTH, POMC cleavage generates 16 kDa fragment (Figure 4A). Antibodies to 16 kDa fragment also recognize intact POMC and its cleavage product, ACTH biosynthetic intermediate (ABI). The amount of 16 kDa fragment stored in the three cell lines at steady state was indistinguishable (Figure 6B). Basal secretion of 16 kDa fragment was unaltered in sh-μ1A wt AtT-20 cells, but $BaCl_2$ stimulated secretion of 16 kDa fragment was reduced by almost a factor of two (Figure 6C).

Analysis of two soluble SG content proteins (POMC and proPC1) supports the conclusion that μ1A plays an essential role in SG maturation in both wt and PAM-1 AtT-20 cells. The fact that basal secretion of processed products of POMC and PC1 was not increased in sh-μ1A cells supports the hypothesis that the vacuolar structures characteristic of sh-μ1A cells are non-condensing SGs. We next turned to PAM-1, a SG membrane protein whose localization is altered when expression of μ1A is reduced, to examine the role of μ1A in granule membrane protein processing.

PAM processing is altered in sh-μ1A PAM-1 cells

When PAM-1 enters immature SGs, it can be cleaved by prohormone convertases; the major cleavage takes place between the two catalytic core domains, forming soluble PHM and PAL membrane (PALm). Cleavage between PAL and the transmembrane domain occurs less frequently, generating soluble PAL (Figure 7A). Unlike soluble SG proteins, PAM-1 and PALm can be retrieved from the regulated secretory pathway; in addition, PAM-1 and PALm that reach the plasma membrane undergo endocytosis and can be returned to the regulated pathway or degraded (8,40). PAM-1 cleavage in non-infected, scramble and sh-μ1A cells was assessed using Western blots and antisera specific for PHM or PAL (Figures 7B and C). The percentage of the total PHM or PAL signal represented by cleaved product (soluble PHM or PALm) was significantly lower in sh-μ1A PAM-1 cells than in non-infected or scramble PAM-1 cells (Figures 7B and C). Although metabolic labeling studies

indicated that PAM-1 was synthesized at similar rates in sh-μ1A and scramble PAM-1 cells, total levels of PAM protein were consistently lower in sh-μ1A PAM-1 cells; increased secretion and increased degradation could each contribute to this difference.

The steady state level of PAM protein reflects newly synthesized PAM-1 trafficking through the biosynthetic pathway along with a substantial amount of PAM that has traversed the endocytic pathway (46). Metabolic labeling was used to assess the trafficking of newly synthesized PAM-1, which must enter the regulated secretory pathway before it can be cleaved to form soluble PHM. Cells incubated in medium containing [^{35}S]Met/Cys for 20 minutes were either collected after 10 min (pulse) or incubated in medium containing unlabeled Met/Cys for 0.5, 1 or 2 hours (chase). PHM-containing proteins were isolated from cell extracts and spent media by immunoprecipitation; following SDS-PAGE, newly synthesized PAM proteins were visualized by fluorography (Figure 7D). The time course over which newly synthesized 120 kDa PAM-1 was converted into PHM was indistinguishable in scramble and sh-μ1A PAM-1 cells (Figure 7E). Data from several metabolic labeling experiments were quantified, supporting the conclusion that access of PAM-1 to the protease that produces PHM was unaltered in sh-μ1A PAM-1 cells (Figure 7F). AP-1A was shown to play a role in the regulated, but not in the basal, release of 63 kDa PC1 and the 16 kDa fragment of POMC. We next evaluated the role of AP-1A in the basal and stimulated secretion of PHM.

Regulated secretion of PHM is impaired in sh-μ1A PAM-1 cells

We used non-infected, scramble and sh-μ1A PAM-1 cells for these studies. As above, we used 2 mM $BaCl_2$ (54) to stimulate secretion from mature SGs (Figure 8A). The sh-μ1A PAM-1 cells secreted about twice as much PHM under basal conditions as non-infected or scramble PAM-1 cells (Figure 8A, boxed graph). Metabolic labeling experiments also indicated that more of the newly synthesized PHM appeared in the medium during the 0–1 h and 0–2 h chase periods in sh-μ1A PAM-1 cells than in scramble PAM-1 cells (Figure 7D). Contributions from newly synthesized PAM-1 in the biosynthetic pathway and from recycled PAM-1 in the endocytic pathway could explain the increase in PHM basal secretion. This result is consistent with the decreased steady state content of PHM observed by Western blot (Figure 7B). The ability of $BaCl_2$ to stimulate the secretion of PHM from mature SGs was reduced by 40% in sh-μ1A PAM-1 cells (Figure 8A).

To determine whether the reduced regulated secretion seen in sh-μ1A PAM-1 cells was due to an impairment in SG maturation, we again turned to metabolic labeling. Based on studies of rat intermediate pituitary and parotid cells, it takes about 2 hours for newly synthesized POMC products and amylase to get to mature SGs (55,56). A metabolic labeling experiment was designed to compare the time at which secretion of newly synthesized PHM produced in scramble vs. sh-μ1A PAM-1 cells became responsive to secretagogue. After the pulse, media were collected every hour for the next 4 hours of chase. After 2 hours of chase, one well received medium containing 2 mM $BaCl_2$ (stim.) while the other well received control medium (basal). After 3 hours of chase, both wells were incubated in basal medium for 1 hour (Figure 8B). PAM proteins were isolated from cells and spent media by immunoprecipitation and newly synthesized PAM proteins were visualized by fluorography.

Secretion of newly synthesized PHM was barely detected during the first collection period. Addition of 2 mM $BaCl_2$ to the 2–3 h chase medium increased PHM secretion by 50% in scramble PAM-1 cells but failed to stimulate secretion of newly synthesized PHM from sh-μ1A PAM-1 cells (Figures 8C and 8D). Taken together, our data suggest that the entry of newly synthesized PHM into secretagogue-responsive granules requires a longer time in sh-μ1A PAM-1 cells than in scramble PAM-1 cells.

The cytosolic domain of PAM interacts with the μ subunit of AP-1A

Since our analysis revealed a role for AP-1A in PAM trafficking, we hypothesized that the cytosolic domain of PAM-1 interacts with AP-1A; the trafficking determinants in this 86 amino acid unstructured region of PAM-1 have been localized to residues 933–950 (Figure 9A) (8). We turned to the yeast two-hybrid system to screen for an interaction between the cytosolic domain of PAM (PAM-CD) and μ1A, μ2, μ3A, μ3B and μ4 (Figure 9B): in this system, PAM-CD interacted only with μ1A. We used several PAM-CD mutants to identify the region responsible for this interaction and to assess its biological relevance (Figure 9C). PAM-1 truncated at residue 961 is trafficked normally and PAM-CD 961s interacted with μ1A. PAM-1 in which the only Tyr residue in the cytosolic domain had been mutated to Ala (Y936A) is endocytosed less rapidly, a process expected to be dependent of AP2 (8); PAM-CD bearing this mutation continued to interact with μ1A. The major trafficking determinants in the cytosolic domain of PAM are located between residues 933 and 950; PAM-CD lacking these residues (Δ933–950) did not interact with μ1A in the yeast two hybrid screen.

In order to determine whether PAM and AP-1A interact *in vivo*, we turned to pituitary, a tissue in which PAM-1 is highly expressed (57). A solubilized particulate fraction prepared from adult mouse pituitary was immunoprecipitated using antibodies to γ-adaptin (Figure 9D) or to the linker region between PHM and PAL (Figure 9E). The availability of an excellent antibody to γ-adaptin and the fact that γ-adaptin (100 kDa), but not μ1A (50 kDa), could be readily resolved from the IgG heavy chain governed the choice of antibody. In both cases, co-immunoprecipitation of PAM-1 and the AP-1A complex was observed. Based on quantification of multiple experiments, 3% of the PAM-1 in pituitary lysates co-immunoprecipitated with γ-adaptin while only 0.6% of the AP-1A co-immunoprecipitated with PAM-1 (graphs in Figures 9D and 9E).

To allow manipulation of the interaction, similar co-immunoprecipitation experiments were conducted using lysates prepared from PAM-1 cells (Figures 9F and 9G). When the γ-adaptin antibody was used to capture the endogenous AP-1A complex, PAM-1 was again co-immunoprecipitated. Although the cytosolic domain of PALm has the same amino acid sequence as the cytosolic domain of PAM-1, PALm was not co-immunoprecipitated by the γ-adaptin antibody. Quantification revealed a significant interaction (graph in Figure 9F). The different behavior of PALm and PAM-1 could reflect their phosphorylation state (58) or a contribution from their luminal domains. Using affinity-purified PAM-1 antibody, γ-adaptin was again co-immunoprecipitated (Figure 9G; quantification shown in graph in Figure 9G). As for the pituitary, about 2% of the total PAM-1 co-immunoprecipitated with γ-adaptin (Figure 9E). Almost 2% of the γ-adaptin co-immunoprecipitated with PAM-1, a higher percentage than observed in pituitary tissue (Figure 9G).

When expressed independently as soluble secretory pathway proteins, both catalytic domains of PAM are efficiently stored in regulated secretory granules (38,40). To determine whether luminal interactions contributed to the co-immunoprecipitation of PAM-1 and AP-1A, we prepared lysates from AtT-20 cells stably expressing PAM-1 899s, which includes the transmembrane domain but only nine of the 86 residues in PAM-CD (Figure 9A, blue arrow). Co-immunoprecipitation of PAM-1 899s with γ-adaptin was observed using antibodies to PAM-1 or γ-adaptin (Figures 10A and 10B). While the PAM-CD/μ1A interaction revealed using the yeast two hybrid assay presumably contributes to the interactions that occur in cells, it is clear that mutations that eliminate the ability of PAM-CD to interact with μ1A in the yeast two hybrid screen are not readily detected by co-immunoprecipitation from cells with a regulated secretory pathway.

We turned to transient transfection of pEAK Rapid cells, a cell line that lacks a regulated secretory pathway, to see if these cells could be used to explore the interactions of μ1A with the cytosolic domain of PAM. Co-immunoprecipitation of endogenous AP-1A with transiently expressed PAM-1 or PAM-1 899s was detected using antibody to PAM (Figure 10C); an exploration of the interaction between the cytosolic domain of PAM and AP-1 will require the use of PAM proteins that lack their luminal domains.

Discussion

The role of AP-1A in SG formation and function

It is striking that a 50% reduction in μ1A levels had such a profound effect on the architecture of the TGN and on SG maturation in AtT-20 corticotrope tumor cells. This could reflect both the role of AP-1A in the trafficking of newly synthesized proteins as they exit the TGN and the role of AP-1A in endocytic trafficking. Formation of clathrin coats on TGN membranes is dependent on close cooperation between AP-1A and GGA proteins (59,60). Lack of this membrane sorting mechanism and membrane proteins normally retrieved after endocytosis may contribute to the breakup of cisternal elements seen in the TGN of sh-μ1A PAM-1 cells. The structure of the Golgi stacks was unperturbed when μ1A levels were reduced.

Ultrastructural analysis indicated that sh-μ1A PAM-1 cells had fewer immature SGs and more vacuolar structures than scramble cells. The fact that cleavage of proPC1, POMC and PAM-1 proceeded normally in sh-μ1A PAM-1 and sh-μ1A wt AtT-20 cells supports the conclusion that these vacuoles are cleavage competent. Based on their appearance, staining for PAM-1 and ACTH and lack of accessibility to an endocytic marker, these vacuolar structures were referred to as non-condensing SGs. They cluster in the mid-region of the cell instead of accumulating at the tips of processes, where mature SGs accumulate (43). In AtT-20 cells, as in pancreatic β-cells and exocrine pancreatic cells, immature SGs have a clathrin-coat which is lost during maturation (10,36,61) and the simplest hypothesis is that non-condensing SGs accumulate when the formation and maturation of SGs is inhibited. The molecular mechanisms involved in condensation are not yet clear, but isolation and examination of these non-condensing SGs may provide insight into the process.

Efficient sorting and packaging of proteins in SGs involves the pH and calcium dependent formation of aggregates and their interaction with TGN membranes of the appropriate composition. With its ability to interact with transmembrane cargo proteins, AP-1A is thought to assist in the sorting of granule membrane proteins into forming vesicles. The accumulation of non-condensing SGs in sh-μ1A PAM-1 cells may be a consequence of the absence of multiple AP-1A cargo proteins. A failure to acidify the lumen or an inability to accumulate calcium could also contribute. Early work on mammotrophs demonstrated interactions between the regulated secretory pathway and the degradative pathway (62). Steady state levels of the products of proPC1 and POMC processing were unaltered in sh-μ1A cells, suggesting that the degradative pathway is not altering the state of the regulated secretory pathway.

Basal secretion of proPC1 and POMC cleavage products was unaltered in sh-μ1A PAM-1 and sh-μ1A wt AtT-20 cells, suggesting that non-condensing SGs are not rapidly released. As SGs mature, their ability to respond to secretagogues increases (34). Our metabolic labeling experiments indicated that it takes longer for the SGs in sh-μ1A PAM-1 cells to become secretagogue responsive than it does for immature SGs in scramble PAM-1 cells. The formation of secretagogue-responsive SGs is known to require the AP-1 mediated removal of VAMP4 and synaptotagmin IV, leaving VAMP2 and synaptotagmin I in mature SGs (34). Consistent with this, $BaCl_2$-stimulated secretion of PHM, ACTH and 63 kDa PC1 was reduced to half in sh-μ1A cells. Mature SGs of normal appearance were located at the tips of cellular processes in sh-μ1A PAM-1 cells. Non-condensing SGs may contain proteins that block their maturation and transport to the tips or processes. Decreased responsiveness to secretagogue, as observed in sh-μ1A PAM-1 cells, is a hallmark of metabolic diseases like diabetes (63,64) and of peptide secreting neuroendocrine tumors (65,66).

The role of AP-1A in PAM-1 and CPD trafficking

Reducing μ1A levels had vastly different effects on PAM-1 and CPD, proteins selected for study because both were known to enter into and be retrieved from immature SGs (5,6,40). PAM accumulated in non-condensing SGs and in mature SGs in sh-μ1A PAM-1 cells. Cleavage of newly synthesized PAM-1 by PC1, which produces PHM and PALm, does not start until PAM-1 enters immature SGs (53); the timing of this event was unaltered in sh-μ1A PAM-1 cells. The ability of its PHM and PAL domains to enter SGs (38) may minimize the need for signal-mediated entry of PAM into immature and non-condensing SGs.

Reducing μ1A levels had a very different effect on endogenous CPD trafficking; instead of its normal localization in TGN cisternae and immature SGs, CPD appeared in small vesicles dispersed throughout sh-μ1A PAM-1 cells. Most notably, CPD and PAM rarely co-localized in sh-μ1A PAM-1 cells. CPD is a major transmembrane glycoprotein in clathrin-coated vesicles in human placenta and rat liver (49). Its cytosolic domain is well conserved and essential for its trafficking (5,6). The cytosolic domain of CPD lacks a canonical AP binding motif, but *in vitro* binding assays revealed that it interacts with AP-1A when phosphorylated by CKII (6).

The different effects of μ1A knockdown on PAM-1 and CPD trafficking may in part reflect the properties of their luminal domains. Membrane and soluble forms of duck CPD have

been expressed in AtT-20 cells (48). About 80% of the membrane form was located at the TGN, with 14% in immature SGs; the soluble form was found in small vesicles (45%) and immature SGs (40%). Metabolic labeling studies indicated that soluble duck CPD was primarily targeted to the constitutive secretory pathway. The entry of membrane CPD into immature SGs seems to require AP-1A. Consistent with our data, down-regulation of μ1A in HeLa cells expressing a CD8/CPD chimera (luminal and transmembrane domains of CD8 linked to the cytosolic domain of CPD) caused its redistribution from the TGN to small vesicles throughout the cell (49).

Although PAM-1 was synthesized at the same rate in sh-μ1A and scramble PAM-1 cells, steady state levels of PAM were reduced in sh-μ1A PAM-1 cells; a detailed evaluation of the endocytic trafficking of PAM-1 in sh-μ1A cells will be required to interpret these observations. The secretion of cleavage products unique to the regulated secretory pathway in the absence of secretagogue, often referred to as constitutive-like secretion (24,67), is a major pathway in AtT-20 cells (53,68). The increased constitutive-like secretion of PHM observed in sh-μ1A PAM-1 cells could be due to a change in PAM trafficking in both the regulated secretory and endocytic pathway. AP-1A/clathrin coated vesicle budding from immature SGs has a well-established role in the retrieval of lysosomal and constitutive membrane proteins from the regulated secretory pathway (67,69). Increased aggregation of POMC and PC1 products would be expected to decrease their entry into budding vesicles (35), accounting for the unaltered constitutive-like secretion of 16K fragment and 63 kDa PC1. The kinetics of constitutive-like secretion suggest the occurrence of an additional sorting step in an endosomal intermediate (70–72), presumably allowing additional sorting for secretion or recycling toward the TGN.

PAM-1 and AP-1A: a novel interaction

The PAM-1/AP-1A interaction described here is not driven by a canonical AP interaction motif. Non-canonical interactions of cargo with AP-2 and AP-4 have been described. The Kir2.3 potassium channel is internalized in clathrin-coated vesicles containing AP-2; mutational analysis revealed a tandem di-hydrophobic motif at its C-terminus that recognizes an α/σ2 interface in AP-2 (73). The cytosolic domain of amyloid precursor protein contains a tyrosine-based signal (YKFFE) that binds to μ4 at a site that is different from that of canonical YXXΦ signals (74). Our findings suggest that AP-1A can also bind non-canonical signals.

Immunoprecipitation of the AP-1A complex pulled down PAM-1 but not PALm. The cytosolic domains of PAM-1 and PALm are identical in amino acid sequence, but differ in phosphorylation status (58,75). While our yeast two-hybrid screen pointed to a role for PAM (933–950), co-immunoprecipitation of the AP-1A complex and a truncated PAM-1 protein lacking its cytosolic domain (PAM-1 899s) revealed an important role for the luminal domains. The proteins that contribute to this interaction have not been identified, but studies using luminal fragments of ATP7A, the P-type ATPase responsible for transporting copper into the lumen of the secretory pathway, demonstrated an interaction with PAM-1 (76). ATP7A localizes to the TGN when copper levels are low, receiving copper from a cytosolic chaperone and delivering it to luminal cuproenzymes like PHM (77). Mutations in the genes

encoding the σ1A (78) or σ1B (79) subunits of human AP-1 result in two developmental disorders, MEDNIK (mental retardation, enteropathy, deafness, peripheral neuropathy, ichthyosis and keratodermia) and Fried syndrome, respectively. Deficiency in σ1A correlates with a defect in copper metabolism recently characterized by abnormal localization of ATP7A (80). The C-terminus of ATP7A contains a dileucine motif that could be recognized by AP-1A and ATP7A recycling from the plasma membrane to the TGN in HeLa cells is AP-1A dependent (81).

Our studies suggest that diminished responsiveness of peptide secreting neurons and endocrine cells may occur in response to minor alterations in AP-1A function. Lack of AP-1A recycling due to reduced levels of *PREPL* alters growth hormone secretion (28). Furthermore, γ-adaptin$^{+/-}$ mice are smaller than wild-type, which could also reflect impaired endocrine function (27). In our study, a modest reduction in μ1A levels in corticotrope tumor cells resulted in vacuolization of the TGN and accumulation of cleavage competent, non-condensing SGs. Although processing of POMC and proPC1 in the regulated secretory pathway proceeded normally, the ability of the cells to secrete stored product in response to secretagogue was substantially diminished. The interaction of AP-1A complexes with membrane proteins known to enter and exit immature SGs is affected by their luminal domains and may not rely only on canonical interaction sites.

Materials and Methods

Antibodies

The antibodies used in this study are summarized in Table 1.

Cell Culture

A mouse corticotrope tumor cell line, AtT-20, was grown at 37°C with 5% CO_2 in Dulbecco's modified Eagle's medium/F-12 (DMEM/F-12) containing 25 mM HEPES, 10% NuSerum, 10% fetal bovine serum, 100 units/ml penicillin, 100 μg/ml streptomycin, and passaged weekly using trypsin. Stably transfected AtT-20 cells expressing wild-type PAM-1 or PAM-1 899s were grown in the same medium and selected using 0.5 mg/ml G418 (8).

Lentiviruses

Wild type AtT-20 cells and stably transfected AtT-20 cells expressing PAM-1 were grown until about 80% confluency and then infected with a lentivirus expressing an shRNA directed against μ1A (Sigma) (Table 2). In parallel, cells were infected with a lentivirus expressing a non-target shRNA (Sigma # SHC002V). At 24 hours post-infection, the medium was removed and cells were selected using growth medium containing 0.4 μg/ml puromycin. In order to obtain lines expressing a constant level of μ1A, cells were subcloned; for each type of cell line, nine to ten clones were used to measure the level of μ1A (Figures 1B and 6A). Three sh-μ1A clones were selected based on their low level of μ1A and three scramble clones were selected based on their unaltered μ1A levels.

Immunofluorescent staining, confocal imaging and image quantification

Cells were plated onto 0.16 to 0.19 mm thick, 12-mm round coverslips (Fisher Scientific) which were coated with 0.1 mg/ml poly-L-lysine for 5 minutes followed by a rinse in NuSerum and two rinses in growth medium. Cells were fixed in 4% formaldehyde in PBS (50 mM NaH_2PO_4, 150 mM NaCl, pH 7.4) for 20 minutes at room temperature. After rinsing in PBS, cells were permeabilized in 0.075% Triton X-100, 2 mg/ml BSA in PBS for 20 minutes at room temperature and then incubated in block buffer (2 mg/ml BSA in PBS) for 20 minutes at room temperature. Primary antibodies diluted in block buffer were incubated with the cells overnight at 4°C. After three rinses in PBS, cells were incubated for one hour in block buffer containing either fluorescein isothiocyanate (FITC, 1:500 dilution) or Cy3 (1:2000 dilution) conjugated donkey antibody to mouse or rabbit immunoglobulin (Jackson ImmunoResearch). After three rinses, coverslips were mounted on slides using ProLong® Gold (Invitrogen). Cells were visualized on a Zeiss LSM 510-Meta using an oil immersion 63X Plan Apochromat objective (NA 1.4). Linescans were done using Metamorph; for both markers, the value with the highest fluorescence intensity value was set to 1. Quantification of fluorescence images was done using Metamorph. Three regions were identified in each cell analyzed: Golgi (based on staining for GM130, TGN38 or PAM), Tip (based on morphology) and Intermediate (non-nuclear, located between the Golgi and a tip, but clearly distinct from each). Supplemental figure 1 identifies the three regions in line scans. For each picture, red and green colors were first separated. Background values were determined by measuring the average intensity in parts of the picture without cells for both green and red images. Background was then subtracted for both green and red images using the average intensity measured as a constant value for the entire image. One to nine 2.5 × 2.5 μm boxes were systematically placed over each region and the average fluorescence signal intensity in each region was measured for 10 to 37 cells. Tip/Golgi and Intermediate/Golgi ratios are shown. Statistical analyses were made using paired t-tests on the ratios calculated.

Electron microscopy

For electron microscopy, cells were fixed with 2.5% glutaraladehyde in 0.1 M cacodylate buffer, scraped and pelleted in gelatin, postfixed with 1% osmium tetroxide and 1.5% potassium ferrocyanide, dehydrated and embedded in an Epon resin. Ultrathin sections were post-stained with uranyl acetate and lead citrate and 30 Golgi complexes in each specimen were systematically sampled and photographed at 6000X with a Jeol JEM-1400 electron microscope equipped with a Gatan Orius SC 1000B bottom mounted CCD-camera. The pictures were viewed at a final magnification of 160,000X. A point grid (82) was overlaid and the volume fractions of the Golgi stack and the TGN were determined by point counting. A line grid was used for measuring the surface to volume ratios of Golgi stack membrane and cisternal membrane in the TGN according to the formula $S/V = 4c/lh$, where c is the number of times the lines intersected the surface of interest, h is the number of times the end points of the lines fell on the structure and l is the length of a test line. Immature granules in the TGN were identified on the basis of their electron dense interior surrounded by an electron lucent halo. Vacuoles/granules in the middle of the cells were counted in the 500 nm peripheral zone of the cytoplasm surrounding the Golgi complex (extending 2.5 μm

in both directions from the point overlying the center of the Golgi complex). All graphs represent the results from 3 experiments. Statistical analyses were made with Student's t-test for the mean values of each experiment (n = 3).

For immunoelectron microcopy, cells were fixed with 4% paraformaldehyde (for PAM staining) or 4% paraformaldehyde + 0.5 % glutaraldehyde (for CPD staining) in 0.1 M phosphate buffer for 2 h, scraped, pelleted and embedded in gelatin. Polyvinylpyrrolidone/ sucrose infiltrated specimens were sectioned at −120°C; sections were collected with methyl cellulose/sucrose, blocked with 1% fish skin gelatin (Sigma) and 1% BSA (Sigma) and incubated with antibody (JH629 diluted 1:200 for PAM; AE142, diluted 1:50 for CPD) for 1 h followed by Protein A conjugated to 10 nm gold particles (University of Utrecht, Utrecht, Netherlands) for 1 h and embedded in uranyl acetate-methyl cellulose. For double staining with ACTH or CPD antibody, PAM was first detected with Protein A/10 nm gold conjugate; the sections were then fixed for 5 min with 1% (for ACTH) or 0.5% (for CPD) glutaraldehyde to block interfering binding, then incubated with antibody to ACTH (antiserum Kathy diluted 1:1000) (42) or CPD (antiserum AE142 diluted 1:50) followed by protein A conjugated to 15 nm gold particles.

For the detection of endosomal uptake cells were incubated with 30 μg/ml peroxidase conjugated wheat germ agglutinin (Sigma) on ice for 30 min, rinsed, chased for 10 min at 37°C and fixed with 1.5% glutaraldehyde in 0.1M phosphate buffer, then incubated with 0.25 mg/ml diaminobenzidine and 0.6 mg/ml hydrogen peroxide for 10 min on ice, rinsed and pelleted as above.

Rescue experiment

pReceiver-M55-mCherry-Ap1m1A was purchased from GeneCopoeia (catalog number: EX-Mm01216-M55; Rockville, MD). In order to create shRNA-resistant mCherry-μ1A (μ1A*), mutations that did not alter the amino acid sequence were introduced using site-directed mutagenesis with the following primer: 5′ CTGTCACCTATCTTGGCCCATGGTGGGGTGAGATTCATGTGGATTAAGCACAAC AACCTGTAC 3′ (T_m = 70.2°C). Scramble and sh-μ1A PAM-1 cells were plated onto 12-mm diameter coverslips (0.16 to 0.19 mm thick, Fisher Scientific) in 24-well dishes; the coverslips were coated with 0.1 mg/ml poly-L-lysine for 5 minutes followed by a rinse in NuSerum and two rinses in growth medium. Two days later, cells were incubated in serum free medium for 30 minutes before being transfected (0.125 μg DNA/well); the Lipofectamine 2000 ® and DNA were mixed in Optimem (Optimem:DNA:Lipofectamine 2000 ® = 200 μl:1 μg: 2.5 μl) and allowed to sit for 25 minutes. After application of the mixture, cells were incubated at 37°C for 6 hours. Transfection medium was then replaced with growth medium and the cells were allowed to recover overnight. Cells were fixed the following day in 4% formaldehyde in PBS and immunostained as described above.

Stimulation of secretion

Cells were plated into 12-well dishes. Secretion experiments were carried out in DMEM/ F-12 air medium containing ITS, 25 mM HEPES, pH 7.4, 50 μg/ml bovine serum albumin (BSA). Cells were equilibrated in air medium during two consecutive 30 minute incubations

at 37°C. Each experiment consisted of a 30 minute incubation in air medium (basal secretion) followed by a 30 minute incubation in either air medium (basal secretion) or in air medium containing 2 mM $BaCl_2$ (stimulated secretion). After each incubation, the medium was centrifuged to remove any non-adherent cells and protease inhibitors were added to the supernatant. After the final incubation, cells were extracted into SDS lysis buffer [0.5% (w/v) SDS, 50 mM Tris, pH 8.0, 1 mM DTT, 2 mM EDTA, 50 mM NaF] containing protease inhibitors.

Biosynthetic labeling

Cells plated into a 4–well dish were equilibrated in DMEM/F-12 air medium as described above for secretion experiments. Cells were incubated in DMEM/F-12 air medium lacking methionine (Met^- medium) for 10 minutes at 37°C before incubation in Met^- medium containing [^{35}S]Methionine/Cysteine protein labeling mix (final activity 1 mCi/ml; PerkinElmer) for 20 minutes. Radioactive medium was removed and replaced with DMEM/F-12 air medium. Cells were either harvested 10 minutes after removal of the radioactive medium (Pulse) or after a 30–240 min incubation in non-radioactive medium (Chase). Cells were lysed in 200 μl of TMT, pH 7.4 containing protease inhibitors. After centrifugation at 8,000 × *g* for 15 minutes, supernatants were used for immunoprecipitation. Medium samples were centrifuged at 2,000 × *g* for 5 minutes and protease inhibitors were added before analysis. To assess labeling efficiency, incorporation of [^{35}S]Methionine/Cysteine into protein was assessed using aliquots (2 μl) of cell extracts and media. Proteins were precipitated by adding 25% tricholoracetic acid (TCA) to 1% of the total cell extract, resuspended in 2% SDS, 0.2M $NaHCO_3$ and added to liquid scintillation fluid for measurement in a scintillation counter. Typically, 1–2 % of the label was incorporated into protein during the 20 min labeling/10 minute pulse.

For immunoprecipitation, affinity-purified PHM antibody (0.8–1 μg) was added to cell extracts, which were incubated at 4°C overnight; after centrifugation for 15 minutes, supernatants were incubated with protein A agarose beads (10 μl packed beads) for 30 minutes at room temperature. Beads were pelleted and washed twice in TMT, pH 7.4 containing protease inhibitors, and once in TM, pH 7.4 containing protease inhibitors. Bound proteins were eluted by incubation for 5 minutes at 95°C in Laemmli sample buffer. Immunoprecipitates were fractionated by SDS-PAGE on 4–15% gradient gels (Bio-Rad). After electrophoresis, gels were incubated in 10% acetic acid, 30% isopropanol for 20 minutes at room temperature, followed by 20 minutes in Enhance (Perkin Elmer) at room temperature. After two rinses in water, the gel was dried and analyzed by fluorography.

Yeast two-hybrid screen

A cDNA fragment encoding the cytosolic domain of rat PAM (PAM-CD; R^{891}WK to PSS^{976}) was inserted into pGBKT7 (Gal4 DNA-binding domain, TRP1). A cDNA encoding medium subunit μ1A, 2, 3A, 3B or 4 was inserted into pACTII (Gal4 Activation Domain, LEU2) as described (83,84). The AH109 yeast reporter strain was grown on Yeast Peptone Dextrose agar plates. Yeast were co-transfected with a PAM-CD plasmid and a medium subunit plasmid; to test the PAM-CD/μ interaction, yeast were grown for 5 days at 30°C on medium lacking leucine, tryptophan and histidine. The growth medium contained 3-

amino-1,2,4-triazole (3-AT), a competitive inhibitor of HIS3, where indicated. Construction of the following mutants was previously described: PAM-CD truncated at residue 961 (961s), PAM-CD with Ala replacing Tyr^{936} (Y936A), PAM-CD lacking residues 933-950 (Δ933-950) (8).

Co-immunoprecipitation

A confluent well of a 6-well dish of AtT-20 cells expressing PAM-1 or a PAM-1 mutant were lysed in 500 μl of 20 mM Na-*N*-Tris[hydroxymethyl]methyl-2-aminoethanesulfonic acid (TES), 10 mM mannitol (TM), 1% Triton X-100 (TMT), pH 6.4, 1 mM EDTA and a cocktail of protease inhibitors (final concentrations 0.34 mg/ml phenylmethylsulfonyl fluoride, 50 μg/ml lima bean trypsin inhibitor, 2 μg/ml leupeptin, 16 μg/ml benzamidine, and 2 μg/ml pepstatin) were added. Cell extracts were centrifuged at 22,000 × *g* for 15 minutes at 4°C. Anterior pituitaries were collected from adult mice and homogenized in TM, pH 6.4 containing 1 mM EDTA and protease inhibitors. Homogenates were centrifuged at 1,000 × *g* for 5 minutes at 4°C to remove cell debris. Particulate material was collected by centrifugation at 435,000 × *g* for 15 minutes at 4°C. Membrane associated proteins were solubilized by suspending this pellet in 250 μl TMT, pH 6.4 containing 1 mM EDTA and protease inhibitors. After incubation at 4°C for 30 min, pituitary lysates were clarified by centrifugation at 22,000 × *g* for 15 minutes at 4°C. Supernatants (250 μl – PAM-1 cells and pituitary cells) were pre-cleared by incubation with 10 μl packed protein A (Repligen BioProcessing) or protein A/G (Thermo Scientific) beads for 30 minutes at 4°C. After centrifugation at 1,000 × *g* for 5 minutes, 10 μl of supernatant was collected as the input for the Western blot and the rest of supernatant was transferred into a new tube containing 1 μg of antibody (affinity-purified rabbit antibody to PAM exon 16 or mouse monoclonal antibody to γ-adaptin); as a control, lysates were incubated with mouse or rabbit immunoglobulin. Samples were tumbled overnight at 4°C and then centrifuged at 22,000 × *g* for 15 minutes at 4°C to remove insoluble material. The supernatants were added to protein A (rabbit antibodies) or protein A/G (mouse antibodies) beads (10 μl packed resin) and tumbled for 1 hour at 4°C. Beads were washed twice in pH 6.4 TMT containing 1 mM EDTA and protease inhibitors, and once in pH 6.4 TM containing 1 mM EDTA and protease inhibitors. The bound fraction was eluted by incubation for 5 minutes at 95°C in Laemmli sample buffer, fractionated by SDS-PAGE on 4–15% gradient gels (Bio-Rad) and subjected to Western blot analysis.

Transfection of pEAK Rapid cells

pEAK Rapid cells (Edge Biosystems, Gaithersburg, MD) a derivative of HEK293 cells, were plated on a 6-well dish which had been coated with 0.1 mg/ml poly-L-lysine for 5 minutes followed by a rinse in NuSerum and two rinses in growth medium. When about 70% confluent, cells were transfected with 1 μg DNA/well using Lipofectamine 2000 ® as described above. After 6 hours, transfection medium was replaced with growth medium; cell extracts were collected the following day for co-immunoprecipitation experiments.

Supplementary Material

Refer to Web version on PubMed Central for supplementary material.

Acknowledgments

We thank Darlene D'Amato and Yanping Wang for their constant technical support. We thank Dr. Kurutihalli Vishwanatha and Megan Miller for their helpful comments on the manuscript. We thank Dr. Lloyd Fricker for his generous gift of carboxypeptidase D antibodies and Dr. Ann Cowan for guidance with our fluorescence imaging experiments. We thank the Electron Microscopy Unit of the Institute of Biotechnology, University of Helsinki for providing laboratory facilities. This work was supported by the National Institutes of Health (DK32949), Scoville Endowment, Janice and Rodney Reynolds Endowment, Liv och Hälsa Foundation, the Magnus Ehrnrooth Foundation, the Perklén Foundation and the Intramural Program of NICHD, NIH.

References

1. Blazquez M, Thiele C, Huttner WB, Docherty K, Shennan KI. Involvement of the membrane lipid bilayer in sorting prohormone convertase 2 into the regulated secretory pathway. Biochem J. 2000; 349(Pt 3):843–852. [PubMed: 10903147]
2. Colomer V, Kicska GA, Rindler MJ. Secretory granule content proteins and the luminal domains of granule membrane proteins aggregate in vitro at mildly acidic pH. J Biol Chem. 1996; 271:48–55. [PubMed: 8550606]
3. Gerdes HH, Rosa P, Phillips E, Baeuerle PA, Frank R, Argos P, Huttner WB. The primary structure of human secretogranin II, a widespread tyrosine-sulfated secretory granule protein that exhibits low pH- and calcium-induced aggregation. J Biol Chem. 1989; 264:12009–12015. [PubMed: 2745426]
4. Stettler H, Beuret N, Prescianotto-Baschong C, Fayard B, Taupenot L, Spiess M. Determinants for chromogranin A sorting into the regulated secretory pathway are also sufficient to generate granule-like structures in non-endocrine cells. Biochem J. 2009; 418:81–91. [PubMed: 18973469]
5. Eng FJ, Varlamov O, Fricker LD. Sequences within the cytoplasmic domain of gp180/carboxypeptidase D mediate localization to the trans-Golgi network. Mol Biol Cell. 1999; 10:35–46. [PubMed: 9880325]
6. Kalinina E, Varlamov O, Fricker LD. Analysis of the carboxypeptidase D cytoplasmic domain: Implications in intracellular trafficking. J Cell Biochem. 2002; 85:101–111. [PubMed: 11891854]
7. Krantz DE, Waites C, Oorschot V, Liu Y, Wilson RI, Tan PK, Klumperman J, Edwards RH. A phosphorylation site regulates sorting of the vesicular acetylcholine transporter to dense core vesicles. J Cell Biol. 2000; 149:379–396. [PubMed: 10769030]
8. Milgram SL, Mains RE, Eipper BA. Identification of routing determinants in the cytosolic domain of a secretory granule-associated integral membrane protein. J Biol Chem. 1996; 271:17526–17535. [PubMed: 8663411]
9. Torii S, Saito N, Kawano A, Zhao S, Izumi T, Takeuchi T. Cytoplasmic transport signal is involved in phogrin targeting and localization to secretory granules. Traffic. 2005; 6:1213–1224. [PubMed: 16262730]
10. Farquhar MG, Palade GE. The Golgi apparatus (complex)-(1954–1981)-from artifact to center stage. J Cell Biol. 1981; 91:77s–103s. [PubMed: 7033246]
11. Boehm M, Bonifacino JS. Genetic analyses of adaptin function from yeast to mammals. Gene. 2002; 286:175–186. [PubMed: 11943473]
12. Hirst J, Barlow LD, Francisco GC, Sahlender DA, Seaman MN, Dacks JB, Robinson MS. The fifth adaptor protein complex. PLoS Biol. 2011; 9:e1001170. [PubMed: 22022230]
13. Robinson MS, Bonifacino JS. Adaptor-related proteins. Curr Opin Cell Biol. 2001; 13:444–453. [PubMed: 11454451]
14. Robinson MS. Adaptable adaptors for coated vesicles. Trends Cell Biol. 2004; 14:167–174. [PubMed: 15066634]
15. Doray B, Kornfeld S. Gamma subunit of the AP-1 adaptor complex binds clathrin: implications for cooperative binding in coated vesicle assembly. Mol Biol Cell. 2001; 12:1925–1935. [PubMed: 11451993]
16. Meyer C, Zizioli D, Lausmann S, Eskelinen EL, Hamann J, Saftig P, von Figura K, Schu P. mu1A-adaptin-deficient mice: lethality, loss of AP-1 binding and rerouting of mannose 6-phosphate receptors. EMBO J. 2000; 19:2193–2203. [PubMed: 10811610]

17. Shih W, Gallusser A, Kirchhausen T. A clathrin-binding site in the hinge of the beta 2 chain of mammalian AP-2 complexes. J Biol Chem. 1995; 270:31083–31090. [PubMed: 8537368]
18. Doray B, Lee I, Knisely J, Bu G, Kornfeld S. The gamma/sigma1 and alpha/sigma2 hemicomplexes of clathrin adaptors AP-1 and AP-2 harbor the dileucine recognition site. Mol Biol Cell. 2007; 18:1887–1896. [PubMed: 17360967]
19. Janvier K, Kato Y, Boehm M, Rose JR, Martina JA, Kim BY, Venkatesan S, Bonifacino JS. Recognition of dileucine-based sorting signals from HIV-1 Nef and LIMP-II by the AP-1 gamma-sigma1 and AP-3 delta-sigma3 hemicomplexes. J Cell Biol. 2003; 163:1281–1290. [PubMed: 14691137]
20. Ohno H, Stewart J, Fournier MC, Bosshart H, Rhee I, Miyatake S, Saito T, Gallusser A, Kirchhausen T, Bonifacino JS. Interaction of tyrosine-based sorting signals with clathrin-associated proteins. Science. 1995; 269:1872–1875. [PubMed: 7569928]
21. Bonnemaison ML, Eipper BA, Mains RE. Role of adaptor proteins in secretory granule biogenesis and maturation. Front Endocrinol (Lausanne). 2013; 4:101. [PubMed: 23966980]
22. Bonifacino JS, Traub LM. Signals for sorting of transmembrane proteins to endosomes and lysosomes. Annu Rev Biochem. 2003; 72:395–447. [PubMed: 12651740]
23. Arvan P, Kuliawat R, Prabakaran D, Zavacki AM, Elahi D, Wang S, Pilkey D. Protein discharge from immature secretory granules displays both regulated and constitutive characteristics. J Biol Chem. 1991; 266:14171–14174. [PubMed: 1860833]
24. Arvan P, Castle D. Protein sorting and secretion granule formation in regulated secretory cells. Trends Cell Biol. 1992; 2:327–331. [PubMed: 14731510]
25. Nykjaer A, Willnow TE. Sortilin: a receptor to regulate neuronal viability and function. Trends Neurosci. 2012; 35:261–270. [PubMed: 22341525]
26. Rousseau K, Kauser S, Pritchard LE, Warhurst A, Oliver RL, Slominski A, Wei ET, Thody AJ, Tobin DJ, White A. Proopiomelanocortin (POMC), the ACTH/melanocortin precursor, is secreted by human epidermal keratinocytes and melanocytes and stimulates melanogenesis. FASEB J. 2007; 21:1844–1856. [PubMed: 17317724]
27. Zizioli D, Meyer C, Guhde G, Saftig P, von Figura K, Schu P. Early embryonic death of mice deficient in gamma-adaptin. J Biol Chem. 1999; 274:5385–5390. [PubMed: 10026148]
28. Radhakrishnan K, Baltes J, Creemers JW, Schu P. Trans-Golgi network morphology and sorting is regulated by prolyl-oligopeptidase-like protein PREPL and the AP-1 complex subunit mu1A. J Cell Sci. 2013; 126:1155–1163. [PubMed: 23321636]
29. Farias GG, Cuitino L, Guo X, Ren X, Jarnik M, Mattera R, Bonifacino JS. Signal-mediated, AP-1/clathrin-dependent sorting of transmembrane receptors to the somatodendritic domain of hippocampal neurons. Neuron. 2012; 75:810–823. [PubMed: 22958822]
30. Burgess J, Jauregui M, Tan J, Rollins J, Lallet S, Leventis PA, Boulianne GL, Chang HC, Le BR, Kramer H, Brill JA. AP-1 and clathrin are essential for secretory granule biogenesis in Drosophila. Mol Biol Cell. 2011; 22:2094–2105. [PubMed: 21490149]
31. Ngo HM, Yang M, Paprotka K, Pypaert M, Hoppe H, Joiner KA. AP-1 in Toxoplasma gondii mediates biogenesis of the rhoptry secretory organelle from a post-Golgi compartment. J Biol Chem. 2003; 278:5343–5352. [PubMed: 12446678]
32. Lui-Roberts WW, Collinson LM, Hewlett LJ, Michaux G, Cutler DF. An AP-1/clathrin coat plays a novel and essential role in forming the Weibel-Palade bodies of endothelial cells. J Cell Biol. 2005; 170:627–636. [PubMed: 16087708]
33. Delevoye C, Hurbain I, Tenza D, Sibarita JB, Uzan-Gafsou S, Ohno H, Geerts WJ, Verkleij AJ, Salamero J, Marks MS, Raposo G. AP-1 and KIF13A coordinate endosomal sorting and positioning during melanosome biogenesis. J Cell Biol. 2009; 187:247–264. [PubMed: 19841138]
34. Eaton BA, Haugwitz M, Lau D, Moore HP. Biogenesis of regulated exocytotic carriers in neuroendocrine cells. J Neurosci. 2000; 20:7334–7344. [PubMed: 11007891]
35. Sobota JA, Ferraro F, Back N, Eipper BA, Mains RE. Not all secretory granules are created equal: Partitioning of soluble content proteins. Mol Biol Cell. 2006; 17:5038–5052. [PubMed: 17005911]
36. Tooze J, Tooze SA. Clathrin-coated vesicular transport of secretory proteins during the formation of ACTH-containing secretory granules in AtT20 cells. J Cell Biol. 1986; 103:839–850. [PubMed: 3017997]

37. Wang Y, Thiele C, Huttner WB. Cholesterol is required for the formation of regulated and constitutive secretory vesicles from the trans-Golgi network. Traffic. 2000; 1:952–962. [PubMed: 11208085]
38. Milgram SL, Johnson RC, Mains RE. Expression of individual forms of peptidylglycine alpha-amidating monooxygenase in AtT-20 cells: endoproteolytic processing and routing to secretory granules. J Cell Biol. 1992; 117:717–728. [PubMed: 1577852]
39. Milgram SL, Kho ST, Martin GV, Mains RE, Eipper BA. Localization of integral membrane peptidylglycine alpha-amidating monooxygenase in neuroendocrine cells. J Cell Sci. 1997; 110 (Pt 6):695–706. [PubMed: 9099944]
40. Milgram SL, Eipper BA, Mains RE. Differential trafficking of soluble and integral membrane secretory granule-associated proteins. J Cell Biol. 1994; 124:33–41. [PubMed: 8294504]
41. Mains RE, Eipper BA. Synthesis and secretion of corticotropins, melanotropins, and endorphins by rat intermediate pituitary cells. J Biol Chem. 1979; 254:7885–7894. [PubMed: 224038]
42. Schnabel E, Mains RE, Farquhar MG. Proteolytic processing of pro-ACTH/endorphin begins in the Golgi complex of pituitary corticotropes and AtT-20 cells. Mol Endocrinol. 1989; 3:1223–1235. [PubMed: 2550814]
43. Matsuuchi L, Buckley KM, Lowe AW, Kelly RB. Targeting of secretory vesicles to cytoplasmic domains in AtT-20 and PC-12 cells. J Cell Biol. 1988; 106:239–251. [PubMed: 2828380]
44. Ciccotosto GD, Schiller MR, Eipper BA, Mains RE. Induction of integral membrane PAM expression in AtT-20 cells alters the storage and trafficking of POMC and PC1. J Cell Biol. 1999; 144:459–471. [PubMed: 9971741]
45. Heldwein EE, Macia E, Wang J, Yin HL, Kirchhausen T, Harrison SC. Crystal structure of the clathrin adaptor protein 1 core. Proc Natl Acad Sci U S A. 2004; 101:14108–14113. [PubMed: 15377783]
46. Back N, Rajagopal C, Mains RE, Eipper BA. Secretory granule membrane protein recycles through multivesicular bodies. Traffic. 2010; 11:972–986. [PubMed: 20374556]
47. Palade G. Intracellular aspects of the process of protein synthesis. Science. 1975; 189:867. [PubMed: 17812524]
48. Varlamov O, Eng FJ, Novikova EG, Fricker LD. Localization of metallocarboxypeptidase D in AtT-20 cells. Potential role in prohormone processing. J Biol Chem. 1999; 274:14759–14767. [PubMed: 10329672]
49. Harasaki K, Lubben NB, Harbour M, Taylor MJ, Robinson MS. Sorting of major cargo glycoproteins into clathrin-coated vesicles. Traffic. 2005; 6:1014–1026. [PubMed: 16190982]
50. Hornby PJ, Rosenthal SD, Mathis JP, Vindrola O, Lindberg I. Immunocytochemical localization of the neuropeptide-synthesizing enzyme PC1 in AtT-20 cells. Neuroendocrinology. 1993; 58:555–563. [PubMed: 8115023]
51. Stettler H, Suri G, Spiess M. Proprotein convertase PC3 is not a transmembrane protein. Biochemistry. 2005; 44:5339–5345. [PubMed: 15807527]
52. Zhou A, Mains RE. Endoproteolytic processing of proopiomelanocortin and prohormone convertases 1 and 2 in neuroendocrine cells overexpressing prohormone convertases 1 or 2. J Biol Chem. 1994; 269:17440–17447. [PubMed: 8021247]
53. Milgram SL, Mains RE. Differential effects of temperature blockade on the proteolytic processing of three secretory granule-associated proteins. J Cell Sci. 1994; 107 (Pt 3):737–745. [PubMed: 8006087]
54. Surprenant A. Correlation between electrical activity and ACTH/beta-endorphin secretion in mouse pituitary tumor cells. J Cell Biol. 1982; 95:559–566. [PubMed: 6292240]
55. Noel G, Mains RE. The ordered secretion of bioactive peptides: oldest or newest first? Mol Endocrinol. 1991; 5:787–794. [PubMed: 1656241]
56. Sharoni Y, Eimerl S, Schramm M. Secretion of old versus new exportable protein in rat parotid slics. Control by neurotransmitters. J Cell Biol. 1976; 71:107–122. [PubMed: 10308]
57. Eipper BA, Myers AC, Mains RE. Peptidyl-glycine alpha-amidation activity in tissues and serum of the adult rat. Endocrinology. 1985; 116:2497–2504. [PubMed: 3996324]

58. Rajagopal C, Stone KL, Francone VP, Mains RE, Eipper BA. Secretory granule to the nucleus: role of a multiply phosphorylated intrinsically unstructured domain. J Biol Chem. 2009; 284:25723–25734. [PubMed: 19635792]
59. Daboussi L, Costaguta G, Payne GS. Phosphoinositide-mediated clathrin adaptor progression at the trans-Golgi network. Nat Cell Biol. 2012; 14:239–248. [PubMed: 22344030]
60. Hirst J, Borner GH, Antrobus R, Peden AA, Hodson NA, Sahlender DA, Robinson MS. Distinct and overlapping roles for AP-1 and GGAs revealed by the “knocksideways” system. Curr Biol. 2012; 22:1711–1716. [PubMed: 22902756]
61. Orci L, Halban P, Amherdt M, Ravazzola M, Vassalli JD, Perrelet A. Nonconverted, amino acid analog-modified proinsulin stays in a Golgi-derived clathrin-coated membrane compartment. J Cell Biol. 1984; 99:2187–2192. [PubMed: 6389572]
62. Smith RE, Farquhar MG. Lysosome function in the regulation of the secretory process in cells of the anterior pituitary gland. J Cell Biol. 1966; 31:319–347. [PubMed: 19866704]
63. Rhodes CJ, Alarcon C. What beta-cell defect could lead to hyperproinsulinemia in NIDDM? Some clues from recent advances made in understanding the proinsulin-processing mechanism. Diabetes. 1994; 43:511–517. [PubMed: 8138054]
64. Taylor R. Type 2 diabetes: etiology and reversibility. Diabetes Care. 2013; 36:1047–1055. [PubMed: 23520370]
65. Meko JB, Norton JA. Management of patients with Zollinger-Ellison syndrome. Annu Rev Med. 1995; 46:395–411. [PubMed: 7598474]
66. Orth DN. Cushing’s syndrome. N Engl J Med. 1995; 332:791–803. [PubMed: 7862184]
67. von Zastrow M, Castle JD. Protein sorting among two distinct export pathways occurs from the content of maturing exocrine storage granules. J Cell Biol. 1987; 105:2675–2684. [PubMed: 3500952]
68. Fernandez CJ, Haugwitz M, Eaton B, Moore HP. Distinct molecular events during secretory granule biogenesis revealed by sensitivities to brefeldin A. Mol Biol Cell. 1997; 8:2171–2185. [PubMed: 9362061]
69. Klumperman J, Kuliawat R, Griffith JM, Geuze HJ, Arvan P. Mannose 6-phosphate receptors are sorted from immature secretory granules via adaptor protein AP-1, clathrin, and syntaxin 6-positive vesicles. J Cell Biol. 1998; 141:359–371. [PubMed: 9548715]
70. Castle JD, Castle AM. Two regulated secretory pathways for newly synthesized parotid salivary proteins are distinguished by doses of secretagogues. J Cell Sci. 1996; 109 (Pt 10):2591–2599. [PubMed: 8923220]
71. Kuliawat R, Arvan P. Protein targeting via the “constitutive-like” secretory pathway in isolated pancreatic islets: passive sorting in the immature granule compartment. J Cell Biol. 1992; 118:521–529. [PubMed: 1639842]
72. Turner MD, Arvan P. Protein traffic from the secretory pathway to the endosomal system in pancreatic beta-cells. J Biol Chem. 2000; 275:14025–14030. [PubMed: 10799475]
73. Ortega B, Mason AK, Welling PA. A tandem Di-hydrophobic motif mediates clathrin-dependent endocytosis via direct binding to the AP-2 alphasigma2 subunits. J Biol Chem. 2012; 287:26867–26875. [PubMed: 22711530]
74. Burgos PV, Mardones GA, Rojas AL, daSilva LL, Prabhu Y, Hurley JH, Bonifacino JS. Sorting of the Alzheimer’s disease amyloid precursor protein mediated by the AP-4 complex. Dev Cell. 2010; 18:425–436. [PubMed: 20230749]
75. Rajagopal C, Stone KL, Mains RE, Eipper BA. Secretion stimulates intramembrane proteolysis of a secretory granule membrane enzyme. J Biol Chem. 2010; 285:34632–34642. [PubMed: 20817724]
76. Otoikhian A, Barry AN, Mayfield M, Nilges M, Huang Y, Lutsenko S, Blackburn NJ. Lumenal loop M672-P707 of the Menkes protein (ATP7A) transfers copper to peptidylglycine monooxygenase. J Am Chem Soc. 2012; 134:10458–10468. [PubMed: 22577880]
77. Gaier ED, Eipper BA, Mains RE. Copper signaling in the mammalian nervous system: synaptic effects. J Neurosci Res. 2013; 91:2–19. [PubMed: 23115049]
78. Montpetit A, Cote S, Brustein E, Drouin CA, Lapointe L, Boudreau M, Meloche C, Drouin R, Hudson TJ, Drapeau P, Cossette P. Disruption of AP1S1, causing a novel neurocutaneous

syndrome, perturbs development of the skin and spinal cord. PLoS Genet. 2008; 4:e1000296. [PubMed: 19057675]

79. Tarpey PS, Stevens C, Teague J, Edkins S, O'Meara S, Avis T, Barthorpe S, Buck G, Butler A, Cole J, Dicks E, Gray K, Halliday K, Harrison R, Hills K, Hinton J, Jones D, Menzies A, Mironenko T, Perry J, Raine K, Richardson D, Shepherd R, Small A, Tofts C, Varian J, West S, Widaa S, Yates A, Catford R, Butler J, Mallya U, Moon J, Luo Y, Dorkins H, Thompson D, Easton DF, Wooster R, Bobrow M, Carpenter N, Simensen RJ, Schwartz CE, Stevenson RE, Turner G, Partington M, Gecz J, Stratton MR, Futreal PA, Raymond FL. Mutations in the gene encoding the Sigma 2 subunit of the adaptor protein 1 complex, AP1S2, cause X-linked mental retardation. Am J Hum Genet. 2006; 79:1119–1124. [PubMed: 17186471]
80. Martinelli D, Travaglini L, Drouin CA, Ceballos-Picot I, Rizza T, Bertini E, Carrozzo R, Petrini S, de LP, El HM, Hubert L, Montpetit A, Torre G, Dionisi-Vici C. MEDNIK syndrome: a novel defect of copper metabolism treatable by zinc acetate therapy. Brain. 2013; 136:872–881. [PubMed: 23423674]
81. Holloway ZG, Velayos-Baeza A, Howell GJ, Levecque C, Ponnambalam S, Sztul E, Monaco AP. Trafficking of the Menkes copper transporter ATP7A is regulated by clathrin-, AP-2-, AP-1-, and Rab22-dependent steps. Mol Biol Cell. 2013; 24:1735–1738. [PubMed: 23596324]
82. Weibel ER, Kistler GS, Scherle WF. Practical stereological methods for morphometric cytology. J Cell Biol. 1966; 30:23–38. [PubMed: 5338131]
83. Aguilar RC, Boehm M, Gorshkova I, Crouch RJ, Tomita K, Saito T, Ohno H, Bonifacino JS. Signal-binding specificity of the mu4 subunit of the adaptor protein complex AP-4. J Biol Chem. 2001; 276:13145–13152. [PubMed: 11139587]
84. Ohno H, Fournier MC, Poy G, Bonifacino JS. Structural determinants of interaction of tyrosine-based sorting signals with the adaptor medium chains. J Biol Chem. 1996; 271:29009–29015. [PubMed: 8910552]
85. Mahaffey DT, Peeler JS, Brodsky FM, Anderson RG. Clathrin-coated pits contain an integral membrane protein that binds the AP-2 subunit with high affinity. J Biol Chem. 1990; 265:16514–16520. [PubMed: 1975814]
86. Francone VP, Ifrim MF, Rajagopal C, Leddy CJ, Wang Y, Carson JH, Mains RE, Eipper BA. Signaling from the secretory granule to the nucleus: Uhmk1 and PAM. Mol Endocrinol. 2010; 24:1543–1558. [PubMed: 20573687]
87. Maltese JY, Eipper BA. Developmental expression of peptidylglycine alpha-amidating monooxygenase (PAM) in primary cultures of neonatal rat cardiocytes: a model for studying regulation of PAM expression in the rat heart. Mol Endocrinol. 1992; 6:1998–2008. [PubMed: 1491686]
88. Yun HY, Johnson RC, Mains RE, Eipper BA. Topological switching of the COOH-terminal domain of peptidylglycine alpha-amidating monooxygenase by alternative RNA splicing. Arch Biochem Biophys. 1993; 301:77–84. [PubMed: 7680192]
89. Husten EJ, Eipper BA. Purification and characterization of PAM-1, an integral membrane protein involved in peptide processing. Arch Biochem Biophys. 1994; 312:487–492. [PubMed: 8037462]
90. Cullen EI, Mains RE. Biosynthesis of amidated joining peptide from pro-adrenocorticotropin-endorphin. Mol Endocrinol. 1987; 1:583–594. [PubMed: 2856410]
91. Song L, Fricker LD. Tissue distribution and characterization of soluble and membrane-bound forms of metallocarboxypeptidase D. J Biol Chem. 1996; 271:28884–28889. [PubMed: 8910535]
92. Dickerson IM, Mains RE. Cell-type specific posttranslational processing of peptides by different pituitary cell lines. Endocrinology. 1990; 127:133–140. [PubMed: 2193796]

Synopsis

Peptides and their processing enzymes leave the *trans*-Golgi network (TGN) in immature secretory granules (SGs). Corticotrope tumor cells were used to explore the role of AP-1A in the generation of secretagogue-responsive mature secretory granules. Reducing levels of the μ1A subunit of AP-1A resulted in a decrease in TGN cisternae and immature SGs and the appearance of vacuolar structures containing cleavage products unique to the regulated secretory pathway (non-condensing SGs). A two-fold reduction in μ1A levels substantially impaired regulated secretion.

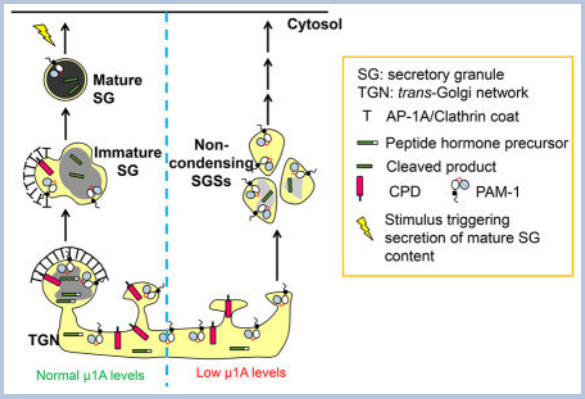

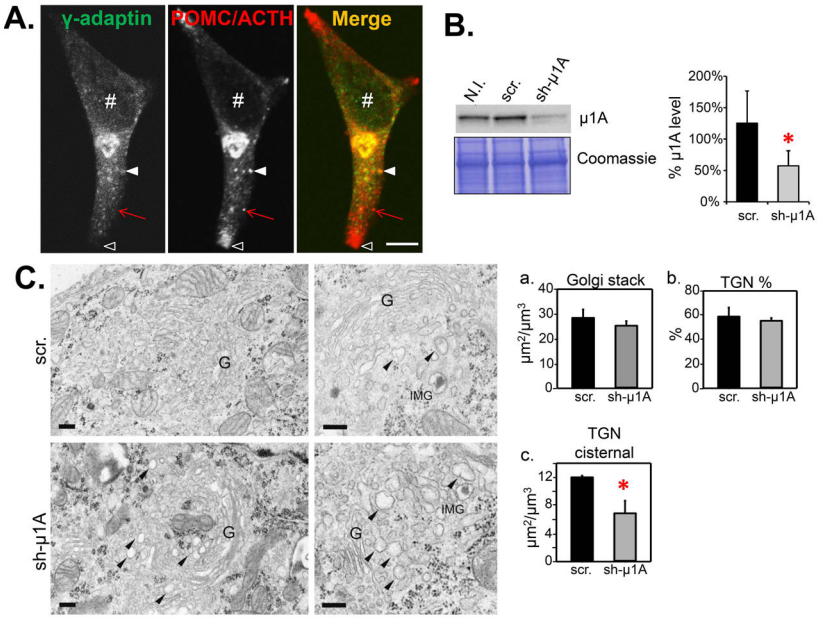

Figure 1. PAM-1 cells expressing reduced levels ofμ1A have a more vacuolated TGN structure

(**A**) Indirect immunofluorescent staining of γ-adaptin (FITC anti-mouse) and POMC/ACTH (Cy3 anti-rabbit) in AtT-20 cells stably expressing PAM-1 (PAM-1 cells); #, nucleus; filled arrowhead, vesicle positive for γ-adaptin and POMC/ACTH; red arrow, vesicle positive for POMC/ACTH but negative for γ-adaptin; open arrowhead, tip of the cell where SGs accumulate; scale bar, 10 μm. Quantification is shown in Supplemental Figure 1C. (**B**) Left, Western blot comparing μ1A expression in non-infected (N.I.) PAM-1 cells, PAM-1 cells infected with a non-target shRNA expressing lentivirus (scramble, scr.) or PAM-1 cells infected with the #549 lentivirus (sh-μ1A); Coomassie staining showed similar amounts of protein in the three cell lines. Right, quantification of μ1A level in nine clones for the scramble PAM-1 cells and ten clones for the sh-μ1A PAM-1 cells. (**C**) Left, Architecture of the Golgi stack and TGN in scramble and sh-μ1A PAM-1 cells. Vacuoles of varying electron density were more frequent in the TGN of sh-μ1A PAM-1 cells (black arrowheads): G, Golgi stack; IMG, immature SG; scale bar, 200 nm. Right, graphs show the surface to volume ratio of Golgi stack membrane (a), the volume fraction of the TGN in relation to the total volume of the Golgi complex (b) and the surface to volume ratio of cisternal elements in the TGN (c) (* $p<0.05$).

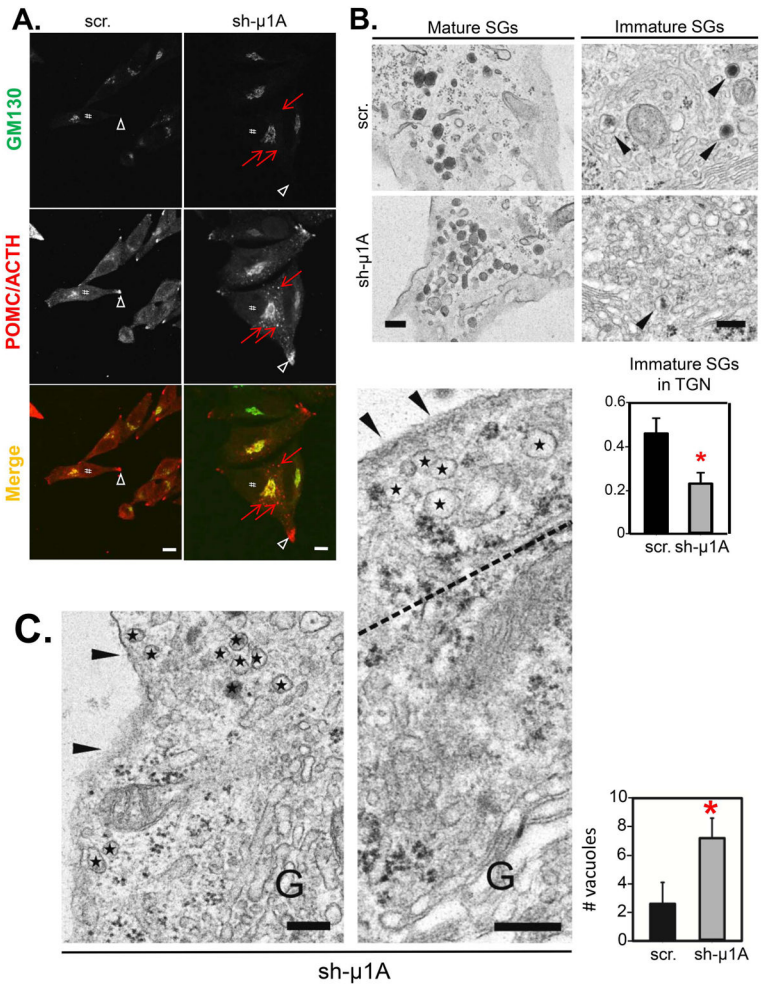

Figure 2. The formation of immature SGs is impaired in sh-µ1A PAM-1 cells

(**A**) Indirect immunofluorescent staining of GM130 (FITC anti-mouse), a *cis*-Golgi marker, and POMC/ACTH (Cy3 anti-rabbit) in scramble and sh-µ1A PAM-1 cell lines; #, nucleus; red arrows, bright puncta positive for POMC/ACTH seen only in sh-µ1A PAM-1 cells; open arrowhead, tip of the cell, where SGs accumulate; scale bar, 10 µm. Quantification of Golgi, intermediate and tip staining is shown in Supplemental Figure 2A. (**B**) Transmission electron micrographs showing mature SGs at the tips of cell processes (left) and immature SGs in the TGN area (black arrowheads, right) in scramble (scr.) and sh-µ1A PAM-1 cells. The graph shows the number of immature SGs in the TGN area (* $p<0.01$). (**C**) Transmission electron micrographs of sh-µ1A PAM-1 cells; black stars mark vacuolar structures located between the Golgi complex and the plasma membrane. Inset: graph shows the number of vacuoles in the 500 nm peripheral zone (between the dashed line and the cell membrane, * $p<0.05$).

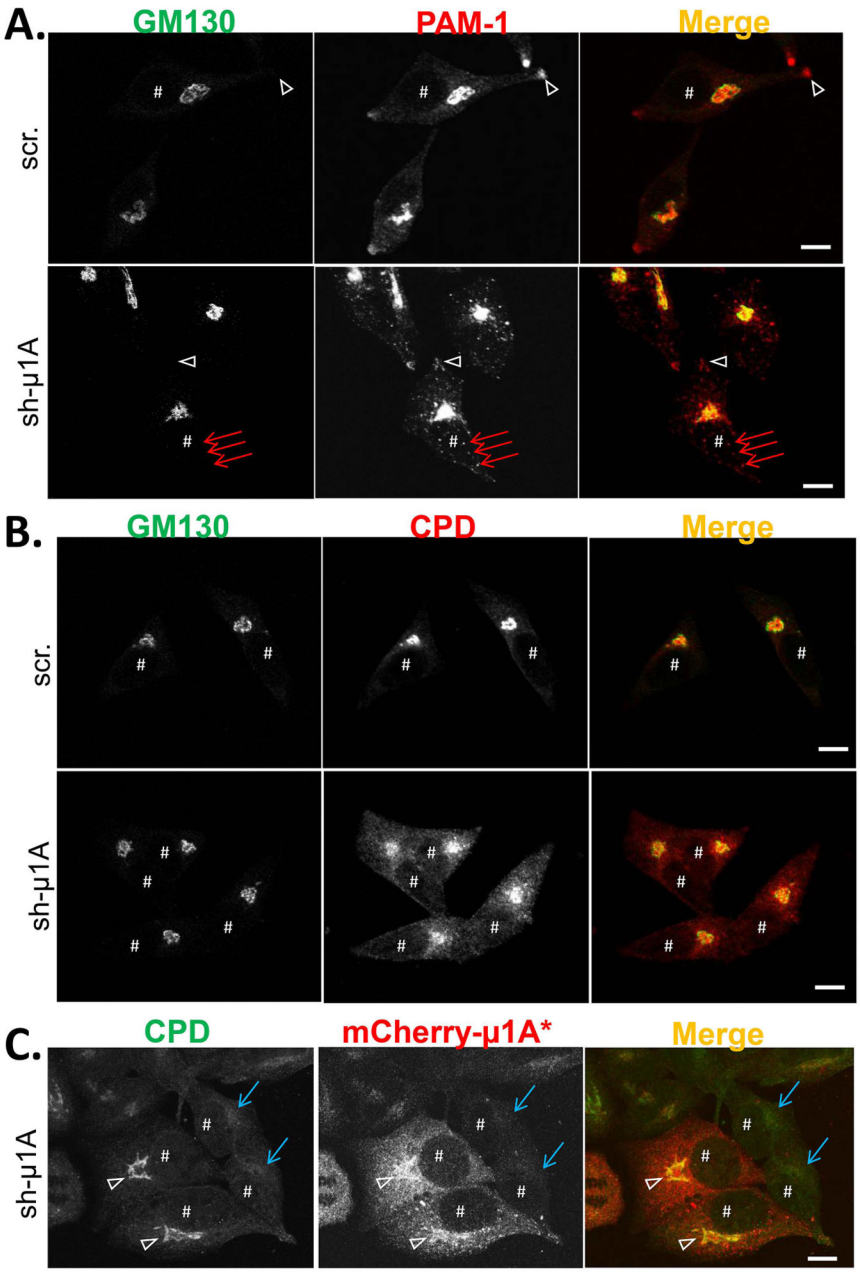

Figure 3. CPD and PAM-1 localization are sensitive to µ1A knockdown

(**A**) Indirect immunofluorescent staining of PAM-1 (C-terminus, Cy3-anti-rabbit) and GM130 (FITC-anti-mouse), a *cis*-Golgi marker, in scramble (scr.) and sh-µ1A PAM-1 cell lines. Red arrows point to bright PAM-1 puncta seen only in sh-µ1A PAM-1 cells. (**B**) Immunofluorescent staining of endogenous CPD and GM130 in scramble and sh-µ1A PAM-1 cells; CPD was visualized using an antibody to its luminal domain (Cy3-anti-rabbit). #, nucleus; open arrowhead, tip of the cell; scale bar, 10 µm. Quantification of Golgi, intermediate and tip staining is shown in Supplemental Figures 2B (PAM) and C (CPD). (**C**) sh-µ1A PAM-1 cells were transiently transfected with plasmid encoding mCherry-µ1A*. Cells were fixed the day following transfection and stained for CPD (FITC-anti-rabbit). Blue

arrows point to non-transfected cells where CPD distribution was diffuse throughout the cell. Open arrowheads point to the Golgi apparatus of transfected cells; CPD was concentrated in the Golgi region, as in scramble PAM-1 cells. Quantification is shown in Supplemental Figure 2D.

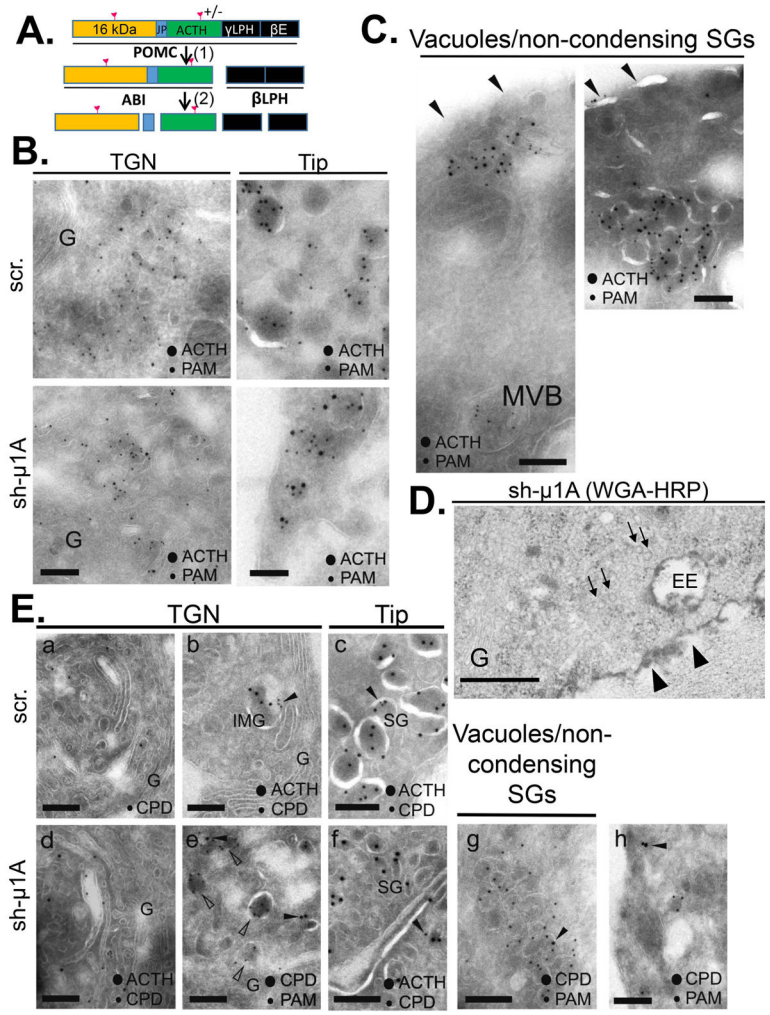

Figure 4. Formation of PAM and ACTH containing vacuoles in sh-μ1A PAM-1 cells

(**A**) Diagram of POMC processing: the cleavage generating ACTH biosynthetic intermediate (ABI) and β-lipotropin (βLPH) starts in the TGN [indicated as (1)] while cleavages producing 16 kDa fragment, joining peptide (JP), ACTH, γ-lipotropin (γLPH) and β-endorphin (βE) occur in SGs [(indicated as (2)] (53). (**B**) ACTH (15 nm gold) and PAM (10 nm gold) co-localized in the TGN and in mature SGs at the tips of scramble and sh-μ1A PAM-1 cells. G, Golgi. (**C**) Cryosections (two panels) of sh-μ1A PAM-1 cells show immunoreactivity for ACTH and PAM in vacuolar/non-condensing SG structures; the PAM-positive multivesicular body (MVB) defines the middle of the cell. Black arrowheads indicate the cell membrane. (**D**) HRP was detected at the plasma membrane (black arrowheads) and in early endosomes (EE) after sh-μ1A PAM-1 cells were incubated in HRP-WGA for 10 min. Black arrows point to non-condensing SGs which lack HRP staining. Scale bar, 500 nm. (**E**) CPD, ACTH and PAM were localized using 15 nm and 10 nm gold as indicated. CPD was present in cisternal and vacuolar elements of the TGN in scramble and sh-μ1A PAM-1 cells (**a**, **d**). Although CPD was found in immature SGs in scramble PAM-1 cells (immature SGs, IMG, identified by ACTH; black arrowhead) (**b**), CPD was largely absent from PAM positive immature SGs or non-condensing SGs in sh-

μ1A PAM-1 cells (**e**, open arrowheads); only one of these structures contained CPD (**e**, upper black arrowhead). CPD was readily identified in TGN membranes (**e**, lower black arrowhead). Very few mature SGs contained CPD (**c**,**f**, black arrowhead). The non-condensing SGs found in sh-μ1A PAM-1 cells contained PAM, but rarely contained CPD (**g**, black arrowhead). Peripheral vesicular or tubular structures usually stained distinctly for CPD or PAM (**h**, black arrowhead). Except for panel D, scale bar, 200 nm.

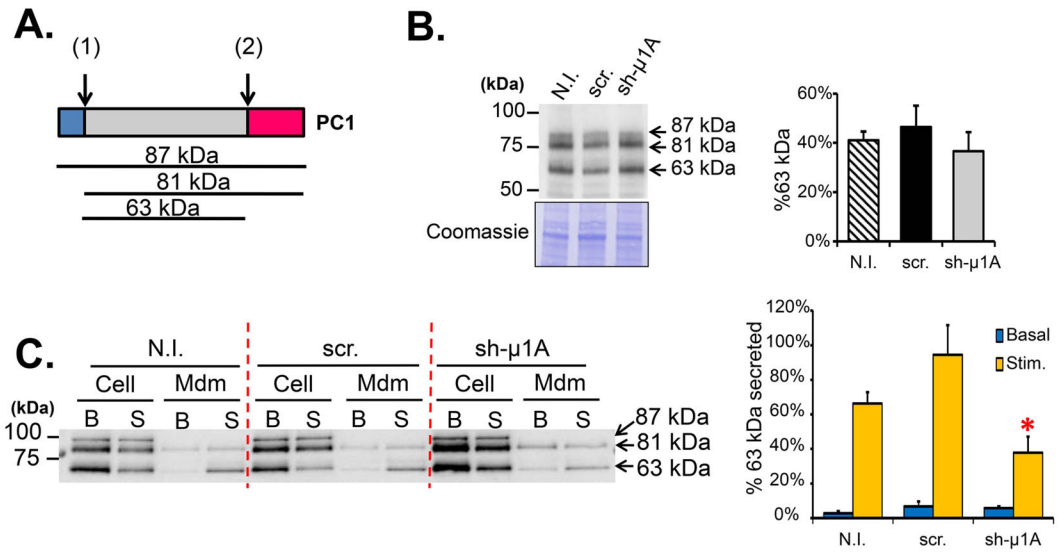

Figure 5. Regulated secretion of soluble content proteins is impaired in sh-µ1A PAM-1 cells

(**A**) Diagram showing the processing of PC1: arrow (1) indicates a cleavage occurring in the endoplasmic reticulum; arrow (2) points to a cleavage happening in mature SGs. (**B**) Left, Western blot of non-infected (N.I.), scramble (scr.) and sh-µ1A PAM-1 cell extracts using a PC1 antibody showed no change in the amounts of PC1 processed products. Coomassie staining showed similar amounts of protein among the three cell lines. Right, quantification of the 63 kDa form of PC1 (63 kDa/(63 kDa + 81 kDa + 87 kDa)) using densitometry (n = 3–8; no statistical differences were seen using a t-test). (**C**) Left, Western blot showing the level of the different forms of PC1 secreted under basal and stimulated conditions in N.I., scr. and sh-µ1A PAM-1 cells. Right, graph showing the secretion rate of the 63 kDa form of PC1 ($63\ kDa_{mdm}/(63\ kDa_{mdm} + 63\ kDa_{cell})$) after densitometry. Four sets of data from two independent experiments are represented in the graphs. (* $p<0.05$)

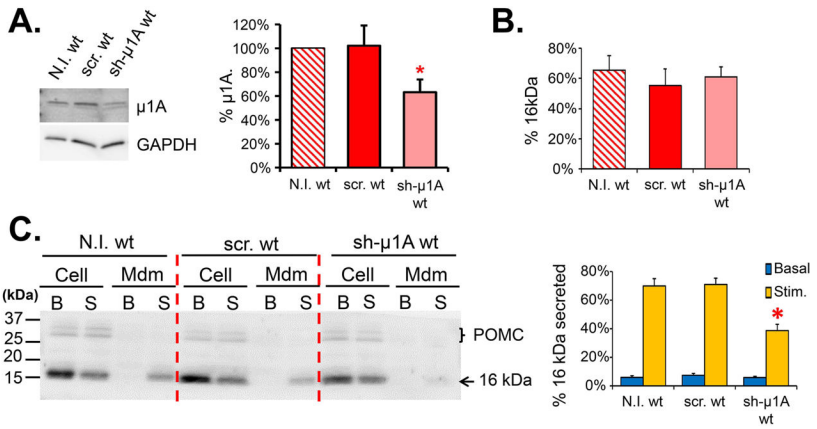

Figure 6. Regulated secretion of soluble content proteins is impaired in wt cells

(**A**) Left, Western blot showing the level of µ1A after infection of wild type (wt) AtT-20 cells with the non-target virus (scr. wt) or with the #549 virus (sh-µ1A wt). Right, quantification of µ1A level of nine sh-µ1A wt clones and ten scramble wt clones relative to µ1A level in non-infected cells (N.I. wt). (**B**) Graph representing the percentage of 16 kDa fragment in all three cell lines (16 kDa/(16 kDa + POMC)). These data were collected by densitometry (n = 5–7; no statistical differences were seen using a t-test). (**C**) Left, Western blot after stimulation of secretion experiment looking at 16 kDa fragment secretion. Right, graph showing 16 kDa fragment secretion rate ($16\ kDa_{mdm}/(16\ kDa_{mdm} + 16\ kDa_{cell})$) after densitometry. Four sets of data from two independent experiments are represented on the graphs (* $p<0.05$ when comparing secretion rate in sh-µ1A wt with N.I.wt and scr. wt cells using a t-test; mdm, medium; B, basal; S, stimulated).

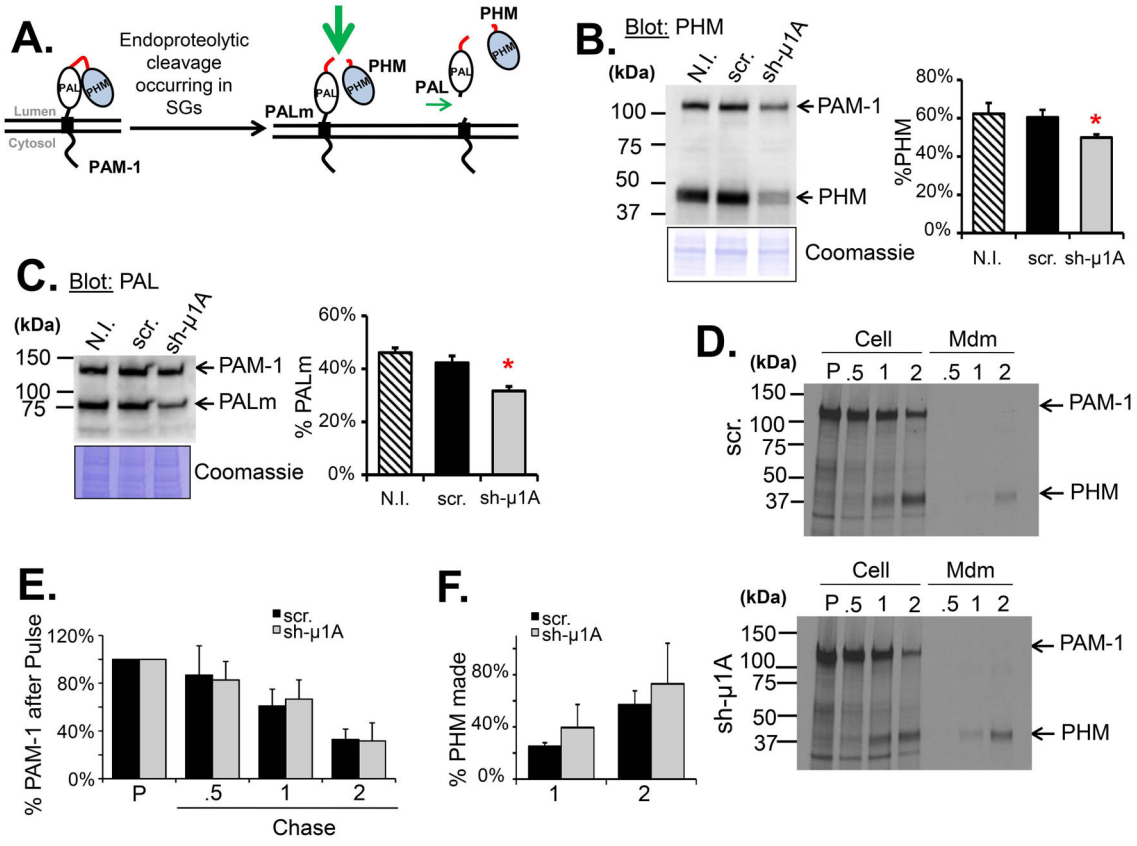

Figure 7. PAM-1 trafficking is altered in sh-µ1A PAM-1 cells

A) Diagram showing the sites at which PAM-1 is cleaved in SGs (green arrow) and the cleavage products created; endoproteolytic cleavage between PHM and PAL occurs more frequently than cleavage between PAL and the transmembrane domain. (**B**, **C**) Left, Western blots of non-infected (N.I.), scramble (scr.) and sh-µ1A PAM-1 cell extracts using a PHM antibody (**B**) or a PAL antibody (**C**). Coomassie staining showed similar amounts of protein among the three cell lines for each blot. Right, quantification of the level of PHM (PHM/(PHM + PAM-1)) (**B**) and PAL (PALm/(PALm + PAM-1)) (**C**) using densitometry (n = 3 for the data shown; * $p<0.05$ from a t-test comparing sh-µ1A values with N.I. and Scr.; no statistical difference was observed between N.I. and scr.). (**D – F**) PAM-1 cells (scramble and sh-µ1A) were incubated in medium containing [^{35}S]Met/Cys for 20 min. PAM-1 cells were either collected 10 minutes later (P) or chased for 0.5, 1 or 2 hours; medium was collected for each chase time. Samples were immunoprecipitated with a PHM antibody and analyzed after fractionation by SDS-PAGE and fluorography. (**D**) Films from two independent experiments were densitized. (**E**) The stability of the newly synthesized PAM-1 was quantified with reference to the amount present after the pulse ([^{35}S]PAM-1$_{chase}$/[^{35}S]PAM-1$_{pulse}$). (**F**) Total PHM synthesis (cells plus medium) from newly synthesized PAM-1 was similar in scramble and sh-µ1A PAM-1 cells (([^{35}S]PHM$_{cell}$ + [^{35}S]PHM$_{mdm}$)/[^{35}S]PAM-1$_{pulse}$).

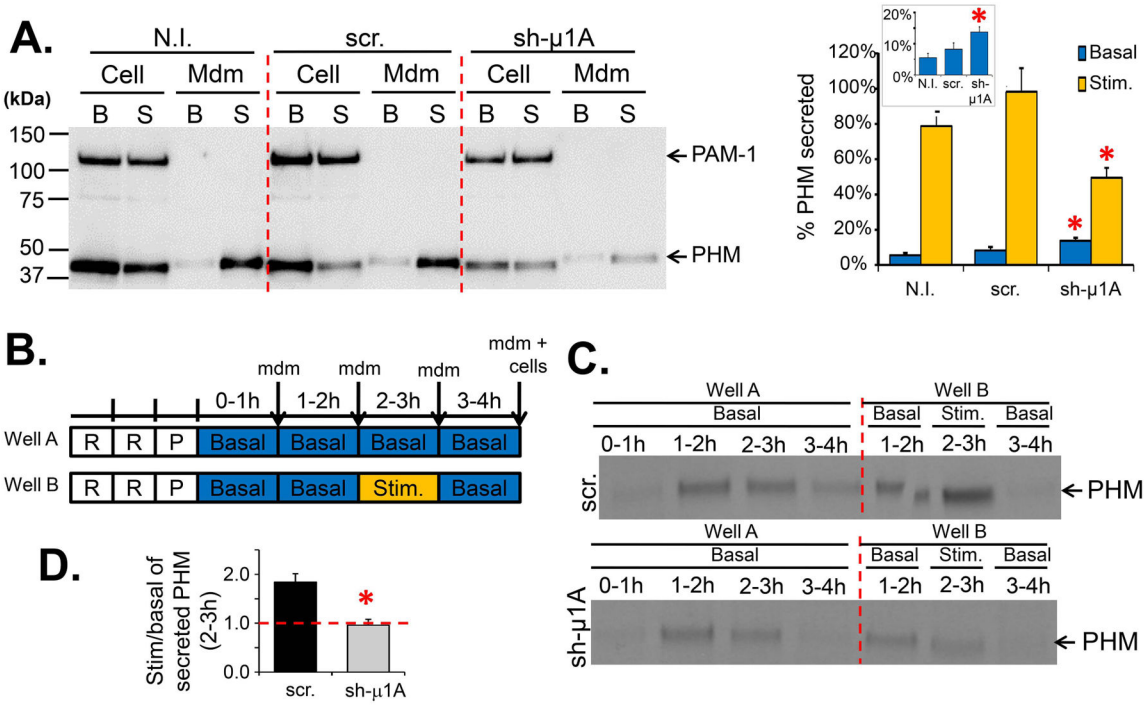

Figure 8. Regulated secretion of PHM is impaired in sh-µ1A PAM-1 cells

(**A**) Left, Western blot showing the level of PHM secreted under basal and stimulated conditions in non-infected (N.I.), scramble (scr.) and sh-µ1A PAM-1 cells. Right, graph showing the secretion rate of PHM ($PHM_{mdm}/(PHM_{mdm} + PHM_{cell})$) after densitometry. Four sets of data from two independent experiments are represented on the graph. Boxed graph shows PHM secretion rate under basal conditions. (**B**) Experimental paradigm for both scramble and sh-µ1A PAM-1 cells: identical wells of cells were rinsed (R) and incubated with [^{35}S]Met/Cys medium for 20 min (P). Spent medium was collected and replaced by basal medium every hour for 4 hours, except during the 2–3 h chase period, when well A received basal medium and well B received secretagogue (stim., basal medium with 2 mM $BaCl_2$). (**C**) Fluorograms showing secretion of newly synthesized PHM purified by immunoprecipitation. (**D**) Graph showing the ratio of newly synthesized PHM secreted under stimulated vs. basal conditions during the 2–3h chase period (mdm, medium; B, basal; S, stimulated; * $p<0.05$).

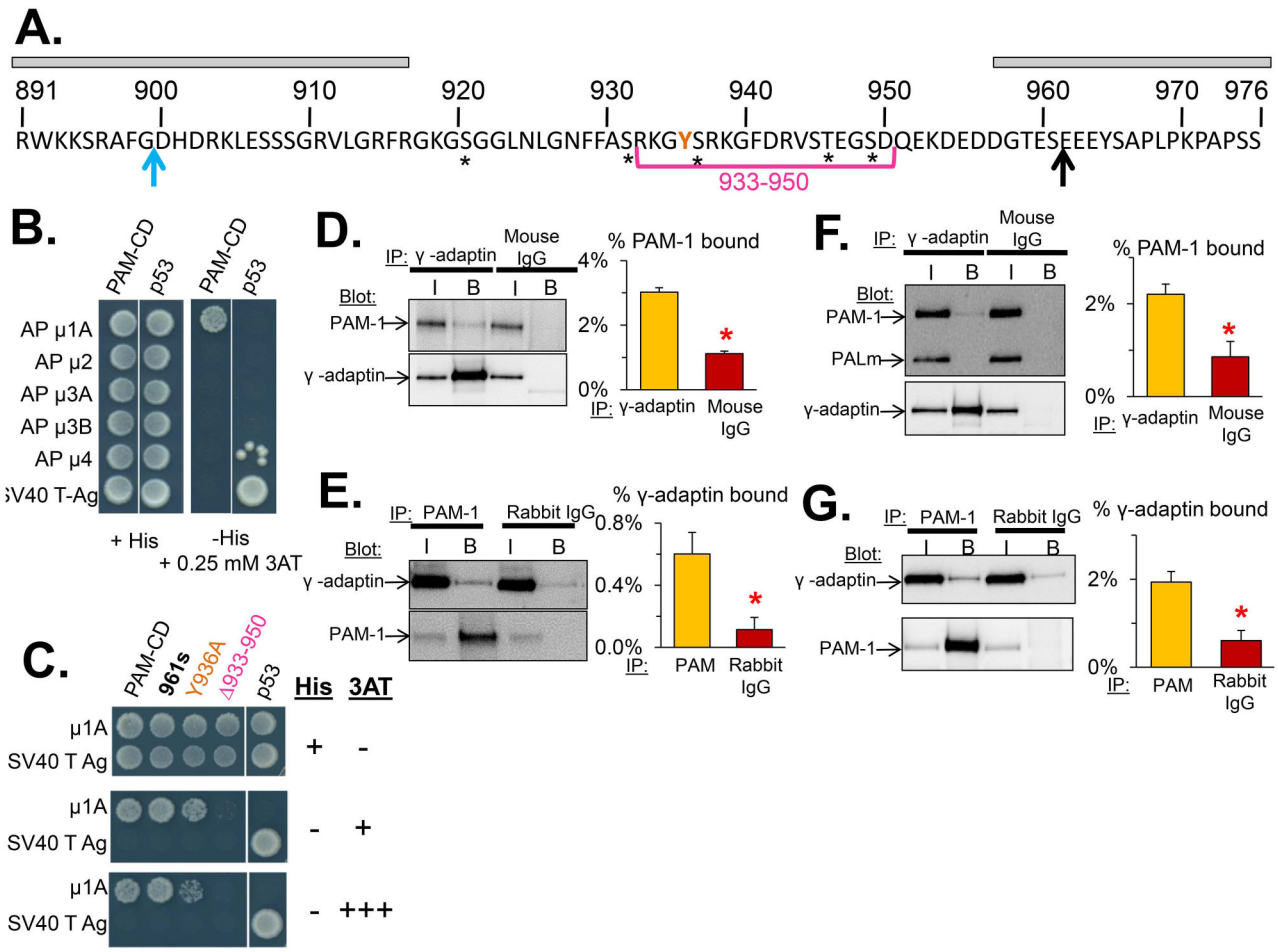

Figure 9. The cytosolic domain of PAM (PAM-CD) interacts with the μ1A subunit of AP-1A

(**A**) Amino acid sequence of the cytosolic domain of PAM. Phosphorylation sites are shown with asterisks. Gray rectangles show regions of PAM-CD which do not alter PAM-1 trafficking upon deletion; striped rectangle shows region involved in trafficking. The blue and black arrows mark residues 899 and 961, respectively. (**B**) Yeast two-hybrid screen for interaction between PAM-CD and the medium subunits of the AP family. Left set, yeast grown in absence of tryptophan and leucine. Right set, yeast grown in absence of tryptophan, leucine and histidine. 3AT, 3-amino-1,2,4-triazole, an inhibitor of histidine synthesis, was used to prevent false positive results. The p53 and SV40 T Ag interaction served as a positive control. (**C**) Yeast two-hybrid screen for interaction of wild-type and mutant PAM-CD with μ1A. Top set, growth of yeast in absence of tryptophan and leucine. Middle and bottom sets, yeast grown in absence of leucine, tryptophan and histidine in presence of increasing amounts of 3AT (+: 0.25 mM 3AT; +++: 1 mM 3AT). Co-immunoprecipitation was used to demonstrate an interaction of PAM-1 and the AP-1A complex in mouse pituitary (**D**, **E**) and in PAM-1 AtT-20 cells (**F**, **G**). Tissue and cell lysates were prepared in TMT, pH 6.4 to preserve the clathrin coat (85). Mouse γ-adaptin antibody was used to capture the AP-1A complex (**D**, **F**) and affinity-purified rabbit antibody directed against the linker region between the PHM and PAL domains of PAM-1 was used to immunoprecipitate PAM-1 (**E**, **G**); mouse and rabbit IgG were used as controls

for background. The amount of input analyzed represents $1/20^{th}$ of the amount of immunoprecipitate analyzed. Quantification of each blot revealed a significant interaction between PAM-1 and AP-1A. I, input; B, bound; n = 4–6; *P<0.05.

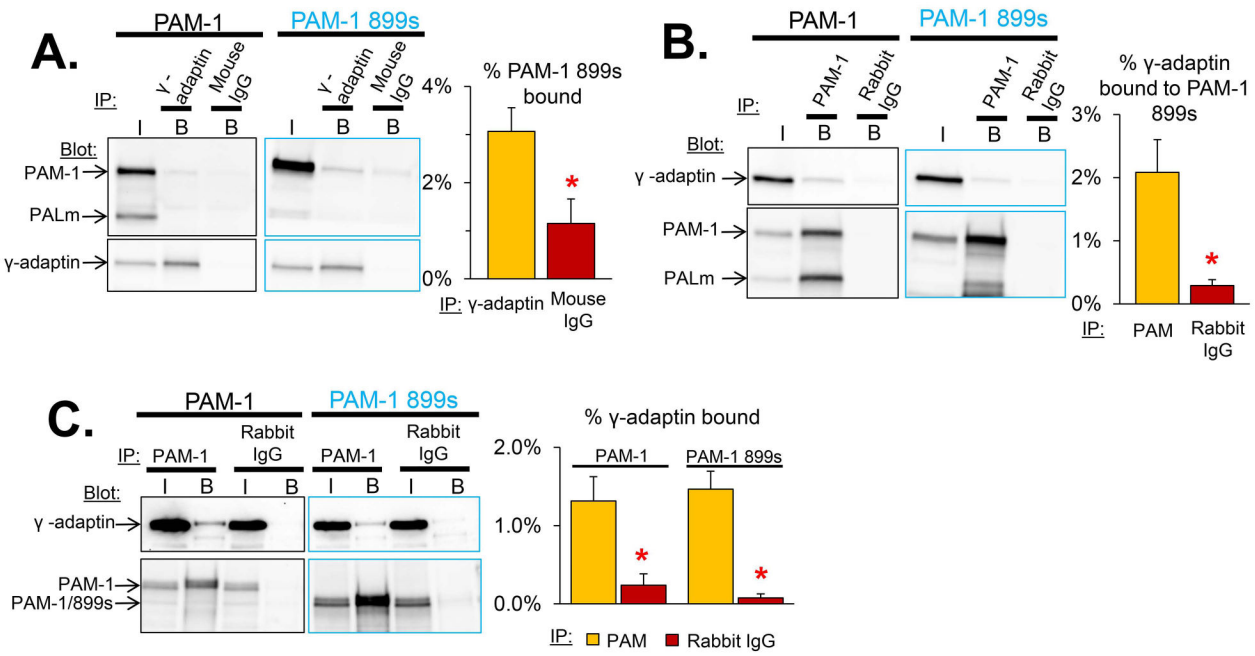

Figure 10. PAM luminal domain contribution to the PAM/AP-1 interaction

(**A**, **B**) Co-immunoprecipitation of PAM and AP-1A was examined in AtT-20 cells expressing PAM-1 or PAM-1 899s (PAM-1 lacking its cytosolic domain) as described in Figure 9. Although it includes only 9 amino acids of the cytosolic domain, PAM-1 899s co-immunoprecipitated with the γ-adaptin antibody (n=4) and γ-adaptin co-immunoprecipitated with the PAM antibody. (**C**) pEAK Rapid cells transiently expressing PAM-1 or PAM-1 899s were analyzed as described for AtT-20 cells. Co-immunoprecipitation was observed using antibody to PAM (n=4).

Table 1

List of antibodies with working dilutions for Western Blot and fluorescent immunostaining along with the source used in this study

Antigen	Working dilution	Identity, Source
rat PAM-1:		
C-STOP, PAM-1(965–976)	1:1000	C-stop (86)
Exon 16, PAM-1(409–497)	1:1000	JH629 (87)
PHM, PAM-1(37–382)	1:1000	JH1761 (88)
PAL, PAM-1(498–604)	1:1000	JH877 (89)
SG proteins:		
PC1(359–373)	1:1000	JH888 (52)
POMC (γ MSH)	1:1000	JH189 (90)
Carboxypeptidase D	1:1000 and see EM	CPD AE142, gift from Dr. Lloyd Fricker (91)
ACTH (Rabbit)	See EM	C-terminus of ACTH (42)
POMC/ACTH (Rabbit)	1:1000	JH93 (N-terminus of ACTH) (92)
AP-1 components:		
μ1A	1:500	ProteinTech Group
γ-adaptin	1:1000	BD Biosciences
Golgi:		
GM130	1:1000	BD Biosciences
TGN38 (155–249)	1:1000	(39)

Table 2

List of viruses clone IDs used in this study.

Clone ID	Name in the study	Target region
TRCN0000111545	545	3′-UTR
TRCN0000111546	546	CDS
TRCN0000111547	547	CDS
TRCN0000111548	548	CDS
TRCN0000111549	549	CDS

3′-UTR: 3′ untranslated region CDS: coding sequence